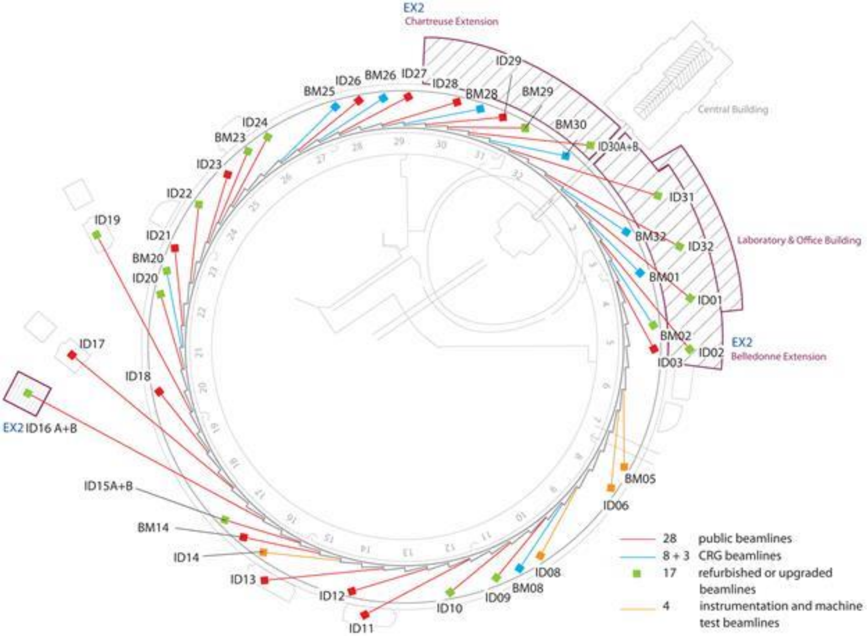

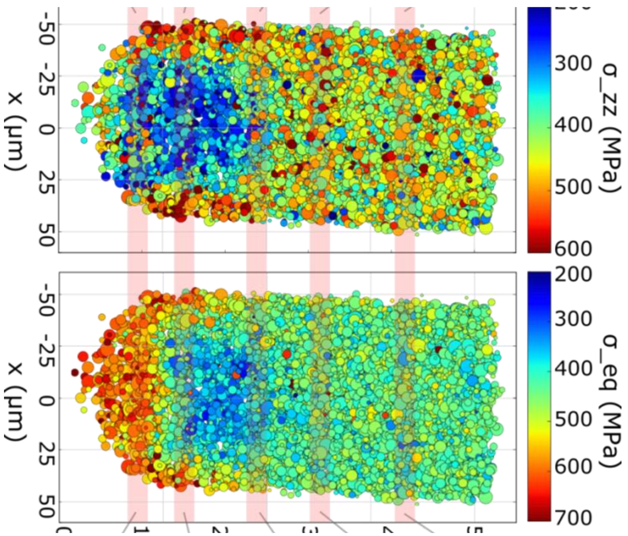

Diffraction based imaging at the Materials Science Beamline

Jon Wright, Wolfgang Ludwig, Pavel Sedmak, Marta Majkut, Carlotta Giacobbe, Thomas Buslaps

ID11 Materials Science beamline : upgraded 2006

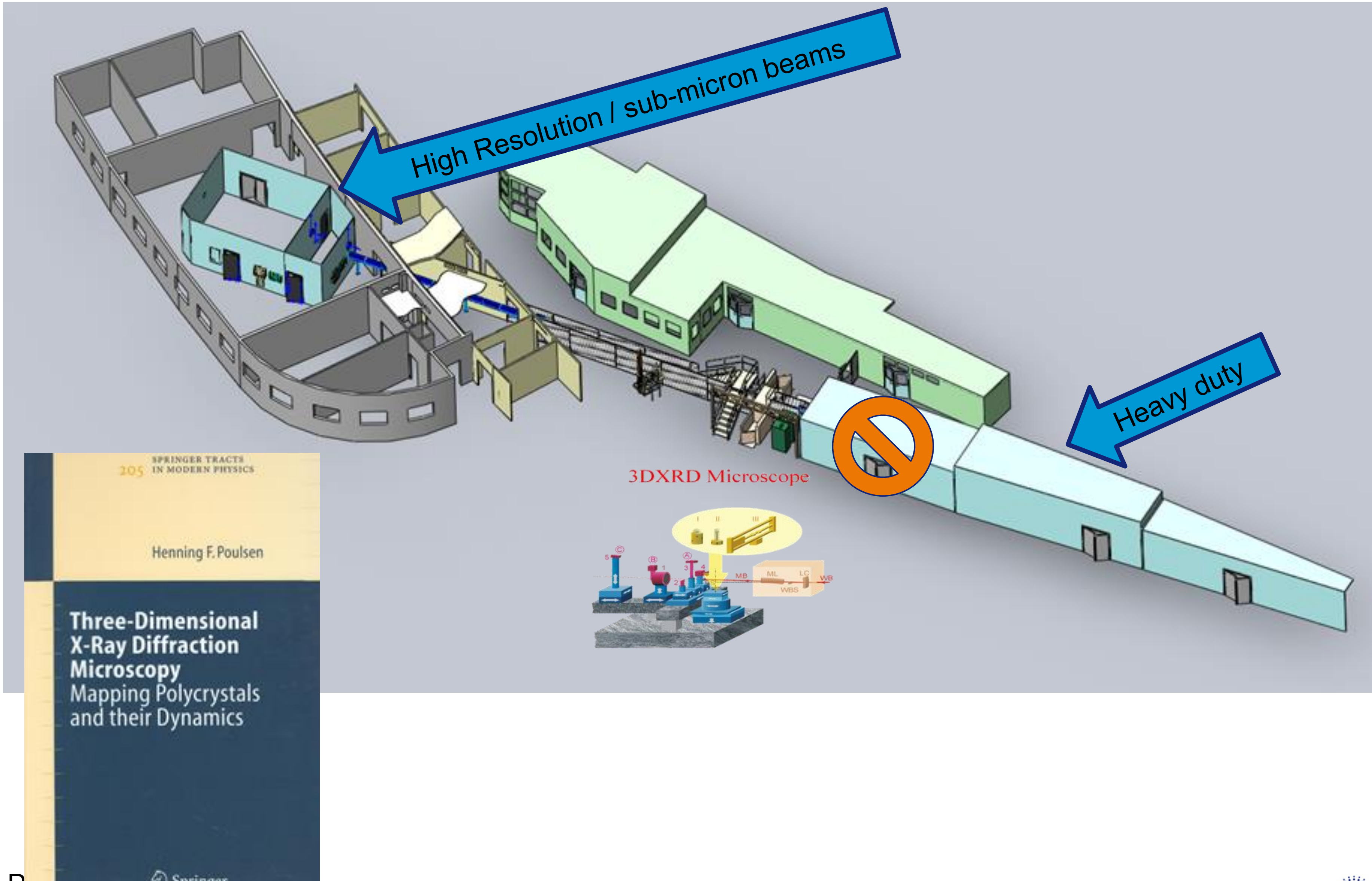

EH1 hutch : Large in-situ experiments

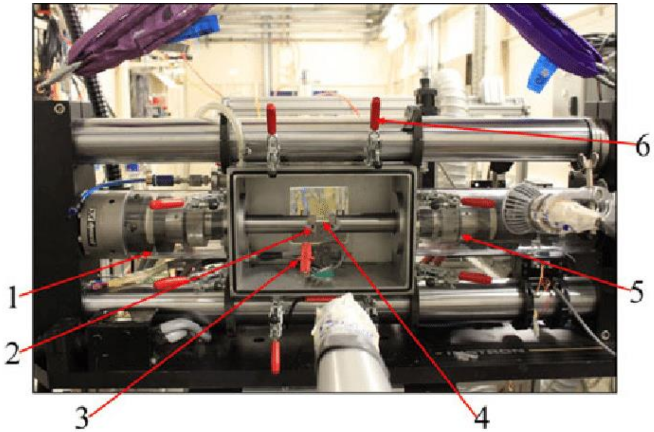

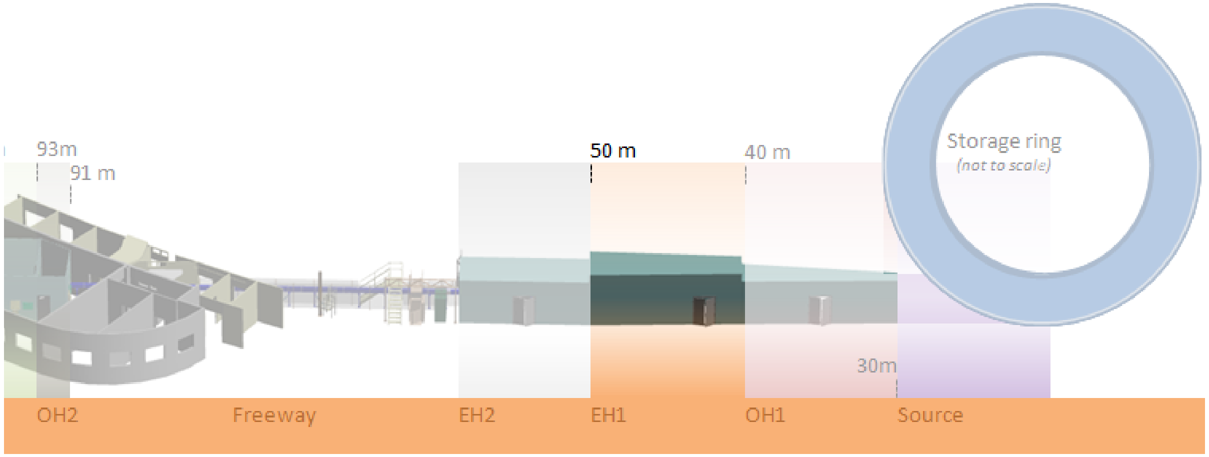

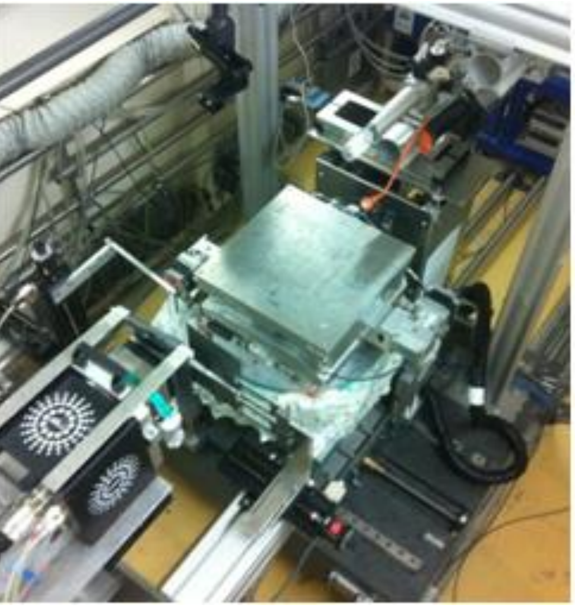

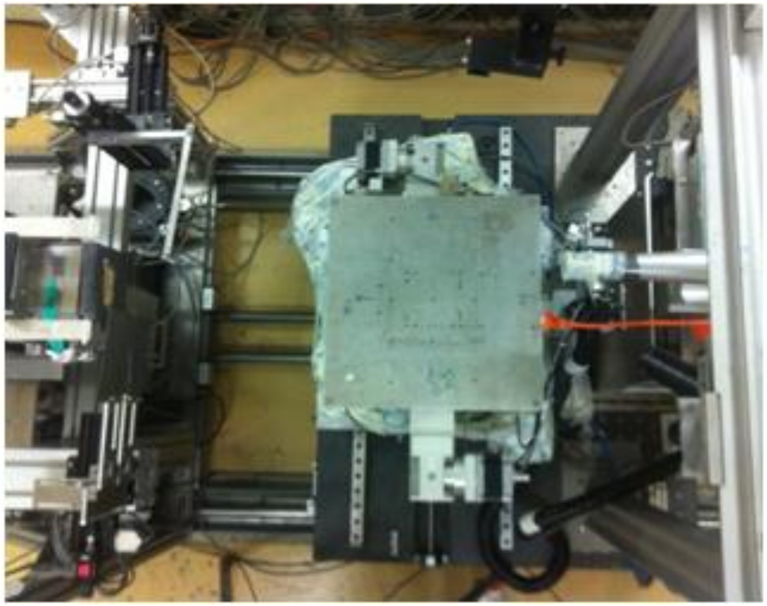

e.g. In-situ levitated, laser heating system

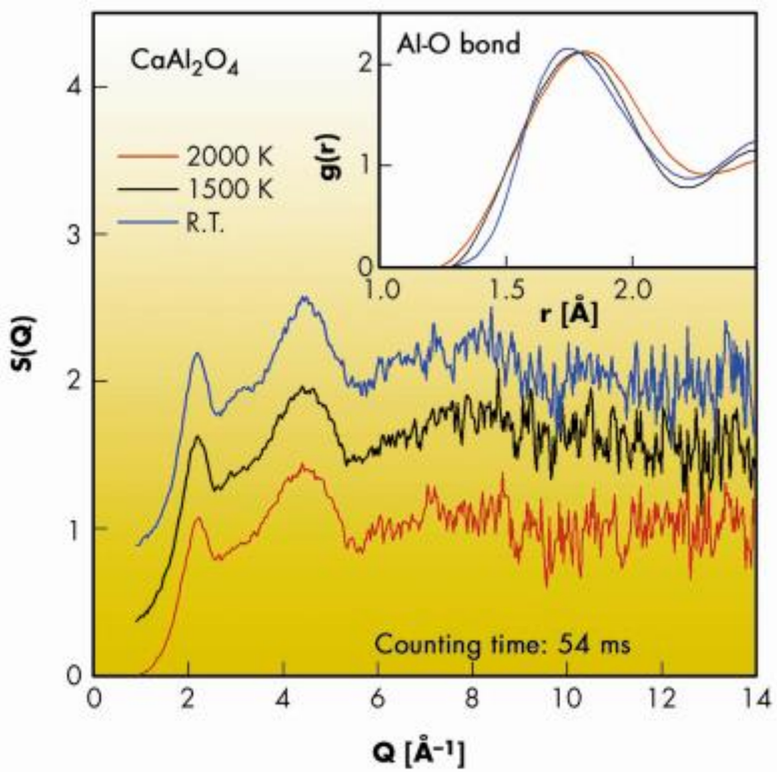

A. Bytchkov (a), L. Hennet (b), I. Pozdnyakova (b), D. Zanghi (b), D.L. Price (b), F. Kargl (c), N. Greaves (c), S. Jahn (d).

(a) ESRF

(b) CRMHT, Orléans (France)

(c) University of Wales, Aberystwyth (UK)

(d) GFZ, Telegrafenberg, Potsdam (Germany)

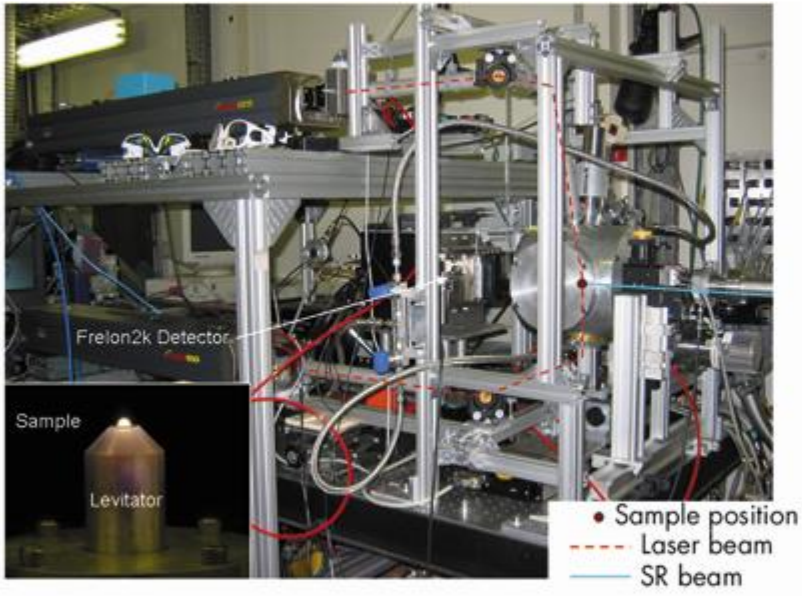

TIME-RESOLVED STRUCTURAL STUDY OF THE GLASS TRANSITION IN GLASS FORMING LIQUIDS

EBS : better statistics at high Q for PDF
Larger Q range

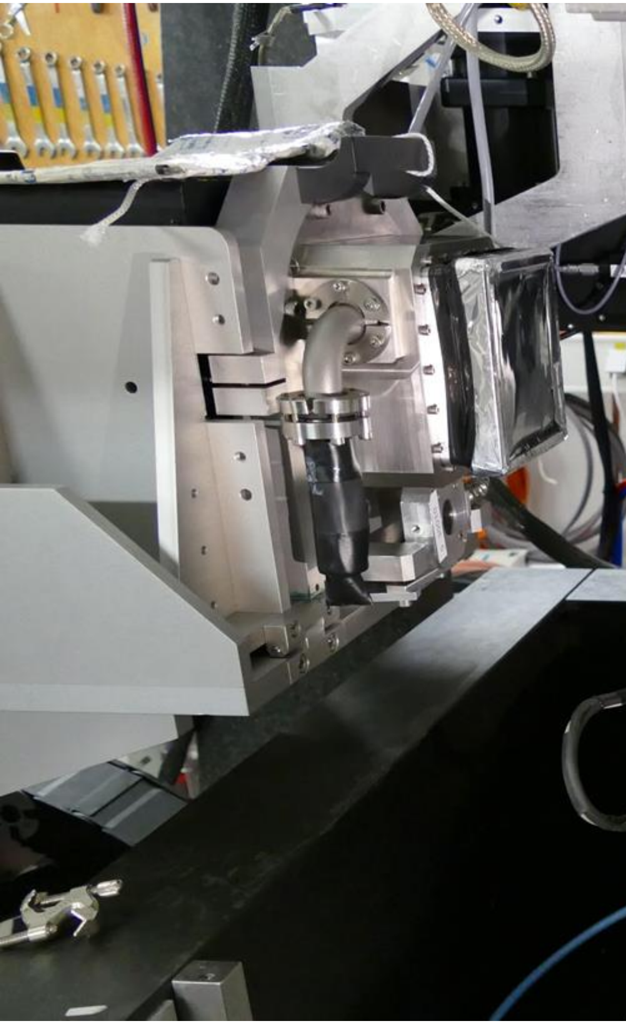

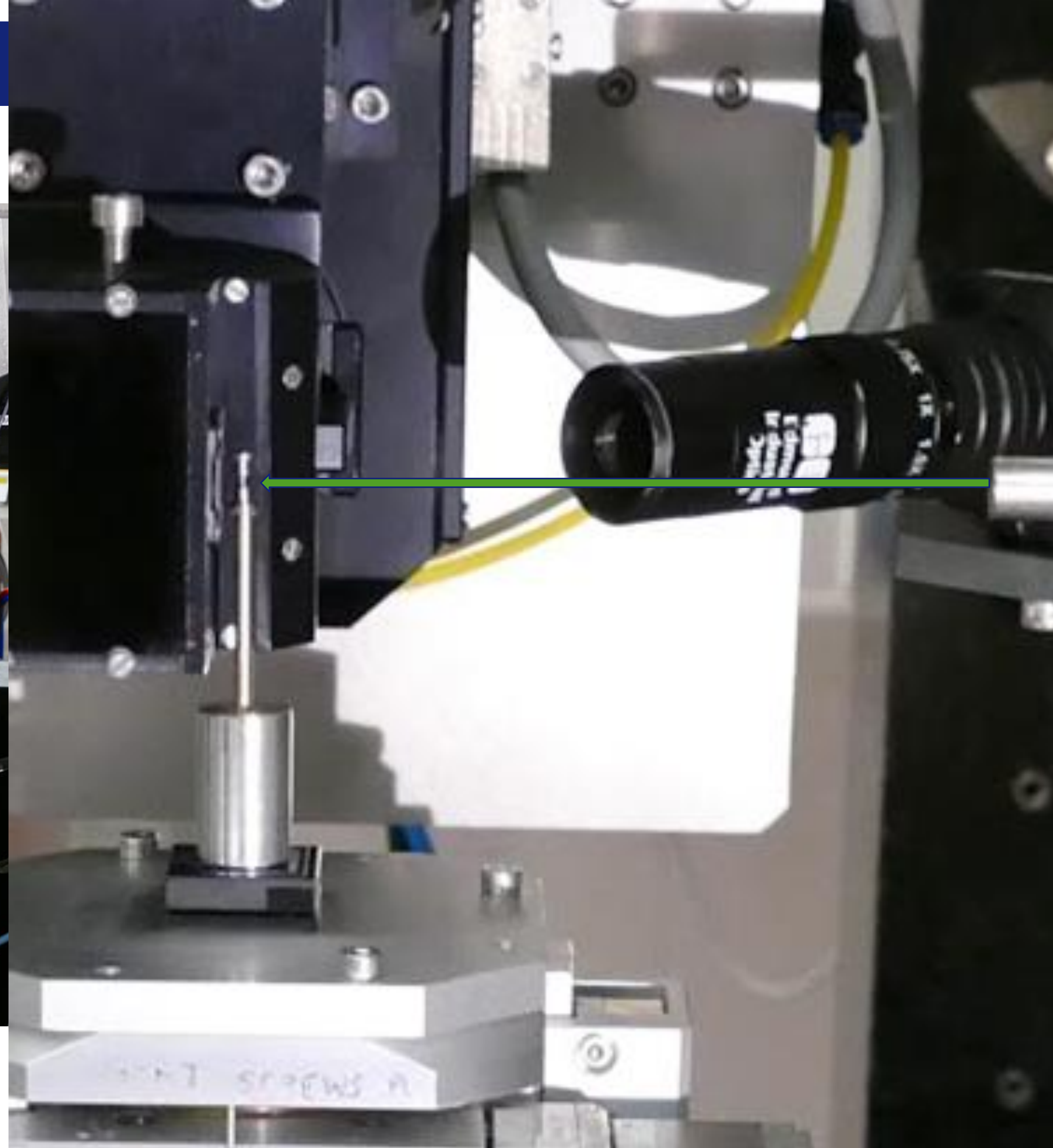

Near-field and far-field detectors

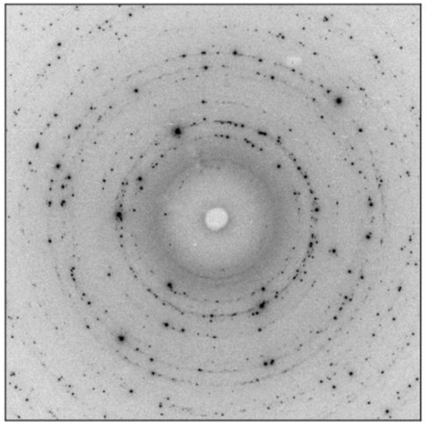

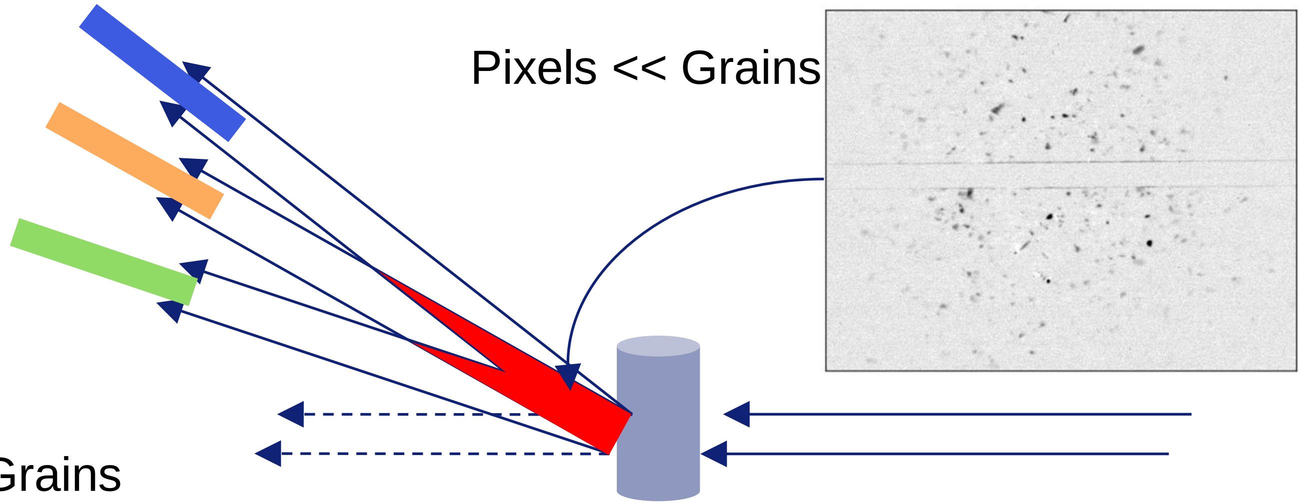

Pixels << Grains

Pixels >> Grains

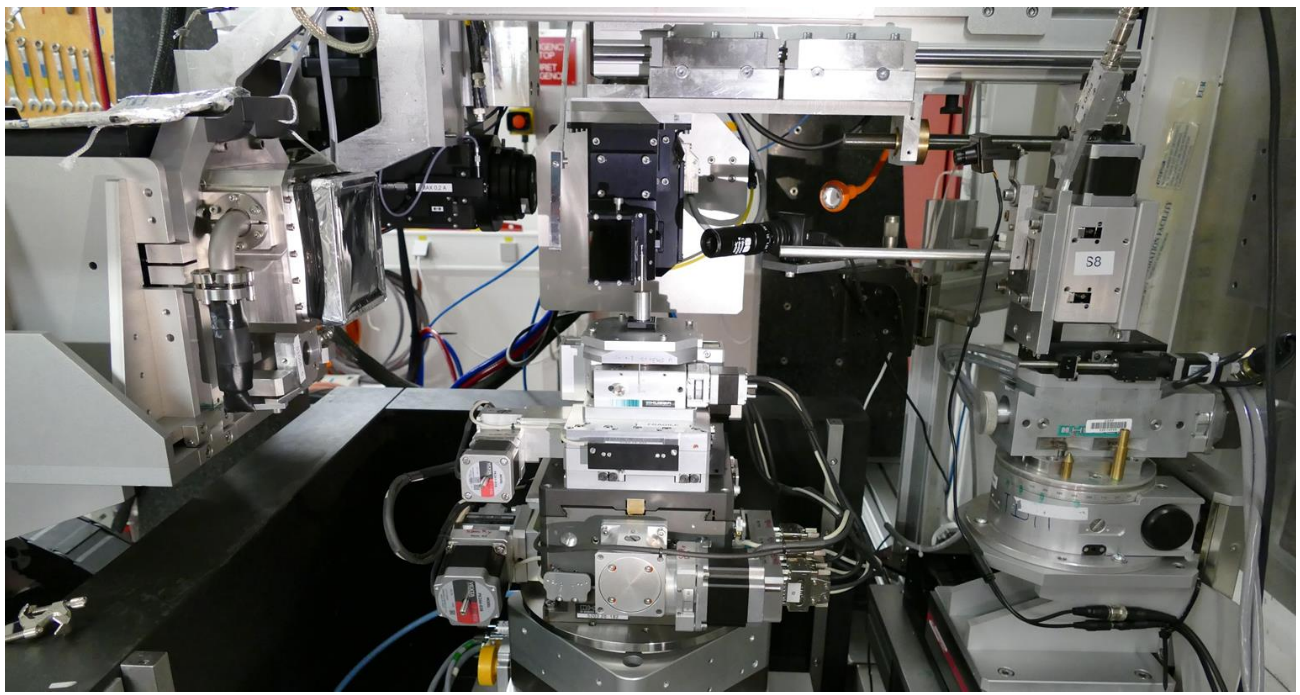

Grain mapping : data processing

Crystallographic information, unit cell + space group are input

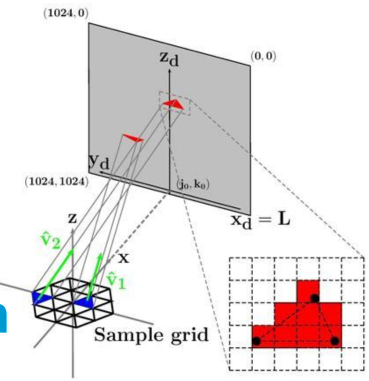

3DXRD :

- **“tracking” principle**
- **Index and reconstruct**
- **2D layers**

Schmidt *et-al*, Riso

HEDM :

- **Forward projection**
- **Supercomputer solves for voxel by voxel orientations**
- **2D layers**

Suter *et-al*, Carnegie Mellon

DCT :

- **Segmentation of spots**
- **“Index” discrete orientations**
- **Reconstruction of 3D volume**

Ludwig *et-al*, INSA Lyon/ESRF

Topo-Tomography :

- **Align on diffraction**
- **Inclined axis**
- **Reconstruct as for computed laminography**

Three-dimensional full-field X-ray orientation microscopy

DCT

Nicola Viganò, Alexandre Tanguy, Simon Hallais, Alexandre Dimanov, Michel Bornert, Kees Joost Batenburg & Wolfgang Ludwig

Scientific Reports **6**, Article number: 20618 | Received: 25 September 2015

Figure 1: Comparison of EBSD surface mapping with the different reconstruction approaches for full-field X-ray orientation microscopy discussed in this work.

From: Three-dimensional full-field X-ray orientation microscopy

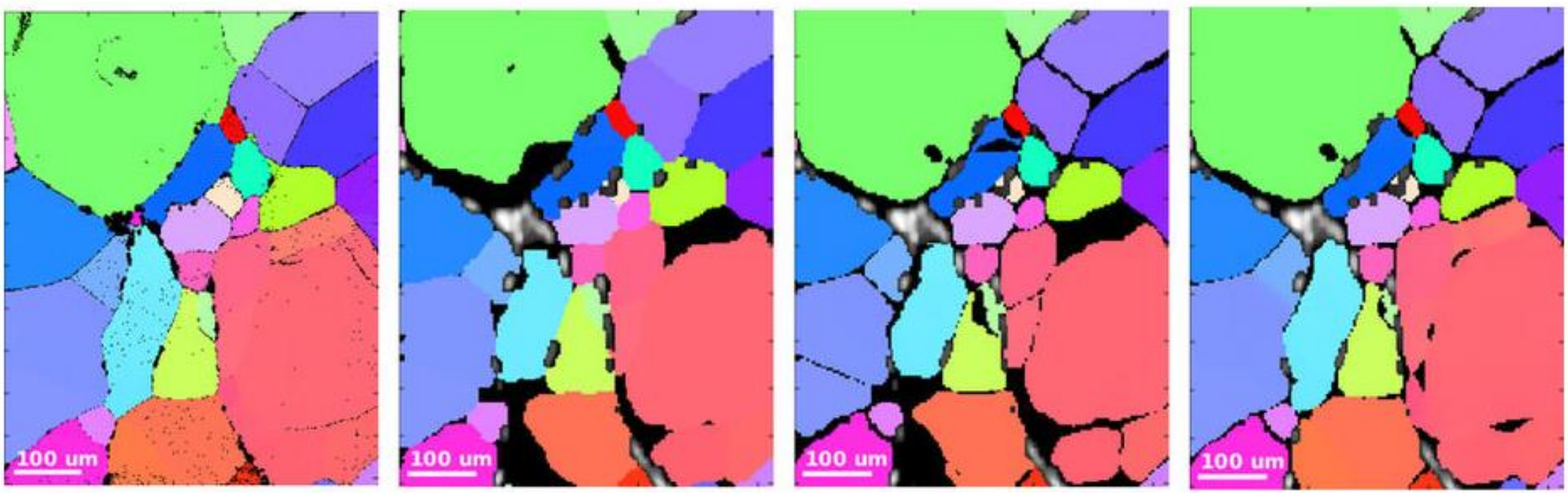

(a) EBSD (b) Dilated DCT-3D (c) DCT-6D (d) DCT-6D + Cluster

DCT - 3D Orientation maps in crystals

EBS :

Better data for deformed materials

Figure 3: Reconstruction of a grain cluster using the extended 6D approach.

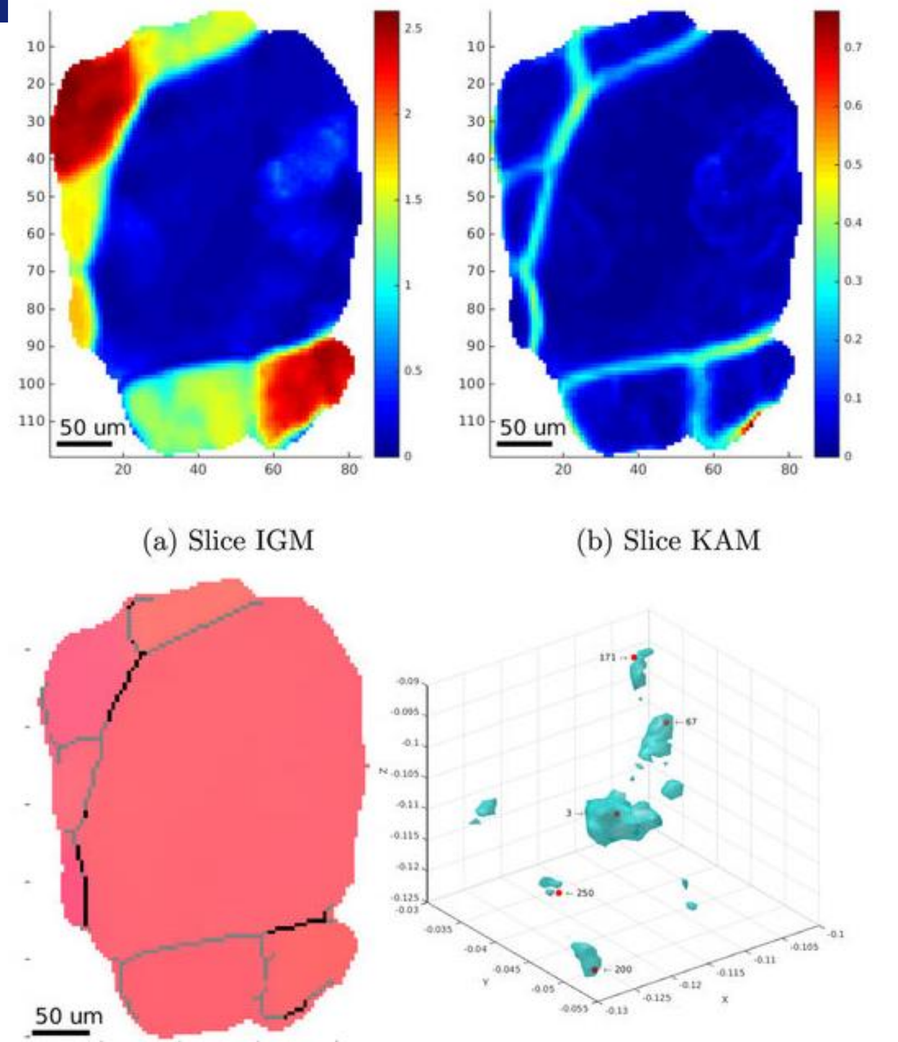

(a) Slice IGM

(b) Slice KAM

(c) IPF

(d) ODF

(**a**–**c**) same slice through the 3D reconstruction showing: (**a**) Intra-granular Misorientation, (**b**) Kernel Average Misorientation (**c**) inverse pole figure colour coding scheme revealing the presence of sub-grains and small angle boundaries from skeletonization of (**a**) (gray: ≥0.5°, black: ≥2°), (**d**) iso-surface of the orientation sub-space reconstructed for the clustered region. Red points indicate sub-grain orientations which had been successfully identified

Figure 2: Comparison of the experimental images for an [2 2 2] reflection at $\theta = 6.21$ *degrees*, $\eta = 112$ *degrees*, with a $\Delta\omega = 6.7$ *degrees* (67 images), with the same forward-projected spot from the result of the reconstruction.

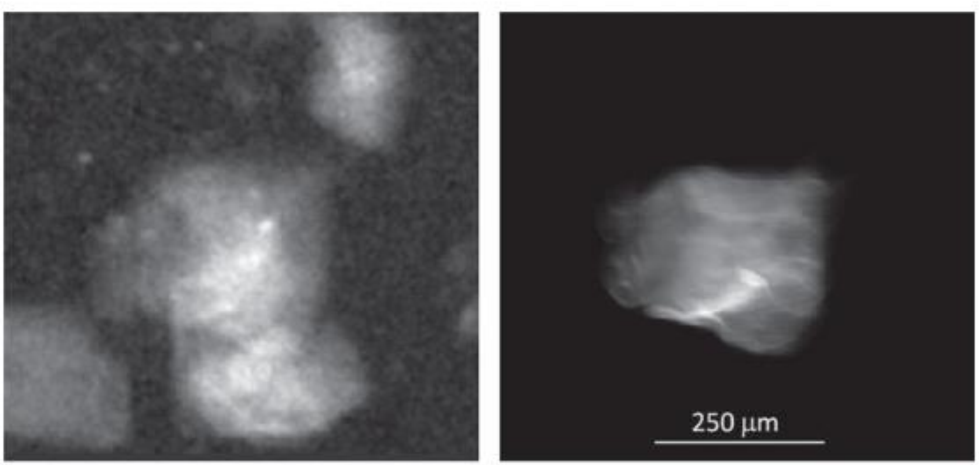

(a) Experimental spot image

(b) Theoretically fwd-projected image

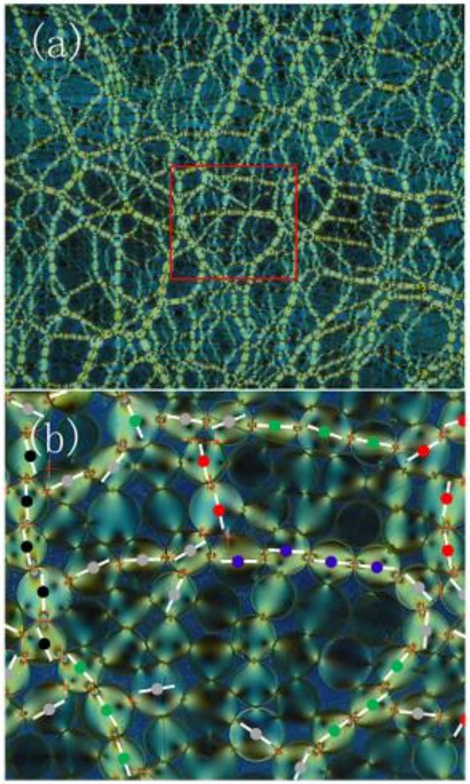

FIG. 2. (Color online) (a) An example of a force-chain network in a 2D layer of granular materials under isotropic compression. Here bidisperse photoelastic disks are used. (b) The portion of panel (a) indicated by the red rectangle, showing several force chains of different lengths using different colors. For example, chains of different lengths are displayed by painting each particle center using dots of different colors: black for length five, blue for length four, green for length three, and red for length two. The short line drawn on top of each particle represents the orientation of the force moment tensor of each particle. Particles with gray-dot centers do not belong to any force chain although satisfying $\sigma_1 \geqslant \langle\sigma_1\rangle$ (see Sec. II for details).

Force-chain distributions in granular systems
Phys. Rev. E **89**, 012203 (2014)
Ling Zhang, Yujie Wang, and Jie Zhang

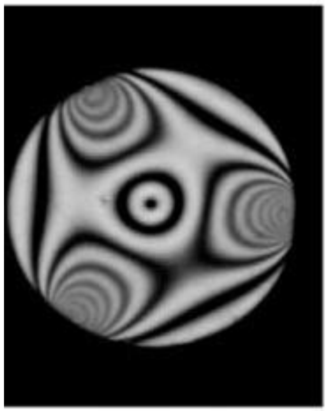

Nature **435**, 1079-1082 (2005)
Contact force measurements and stress-induced anisotropy in granular materials
T. S. Majmudar & R. P. Behringer

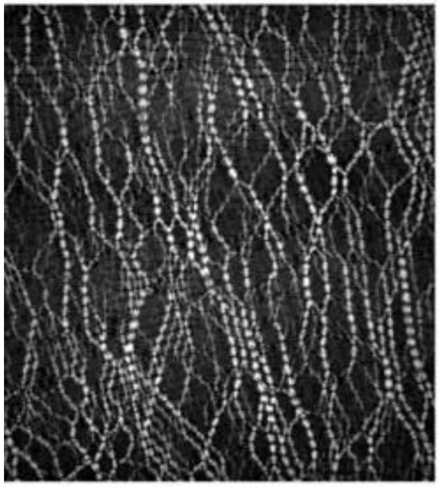

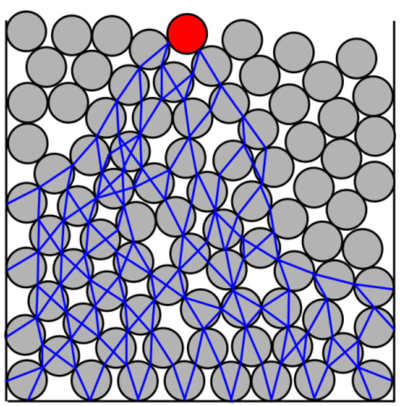

Natural sand grains

Granular Matter (2011) 13:251–254
DOI 10.1007/s10035-011-0251-x

ORIGINAL PAPER

Can intergranular force transmission be identified in sand?

First results of spatially-resolved neutron and X-ray diffraction

Stephen A. Hall · Jonathan Wright · Thilo Pirling ·
Edward Andò · Darren J. Hughes ·
Gioacchino Viggiani

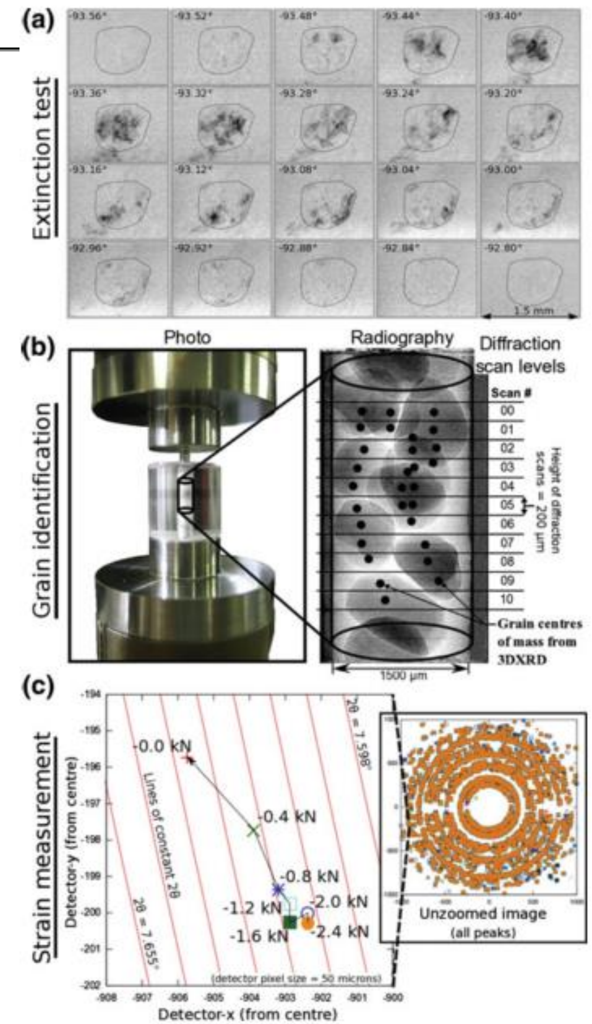

Promising results but the natural sand grains showed significant internal structures (twins and cracks). On loading the internal domains move with respect to each other.

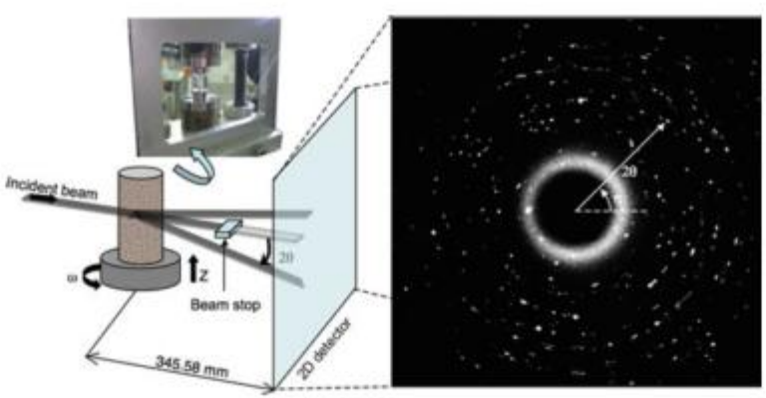

Larger system – Collaboration with Steve Hall, Ryan Hurley, Jose Andrade

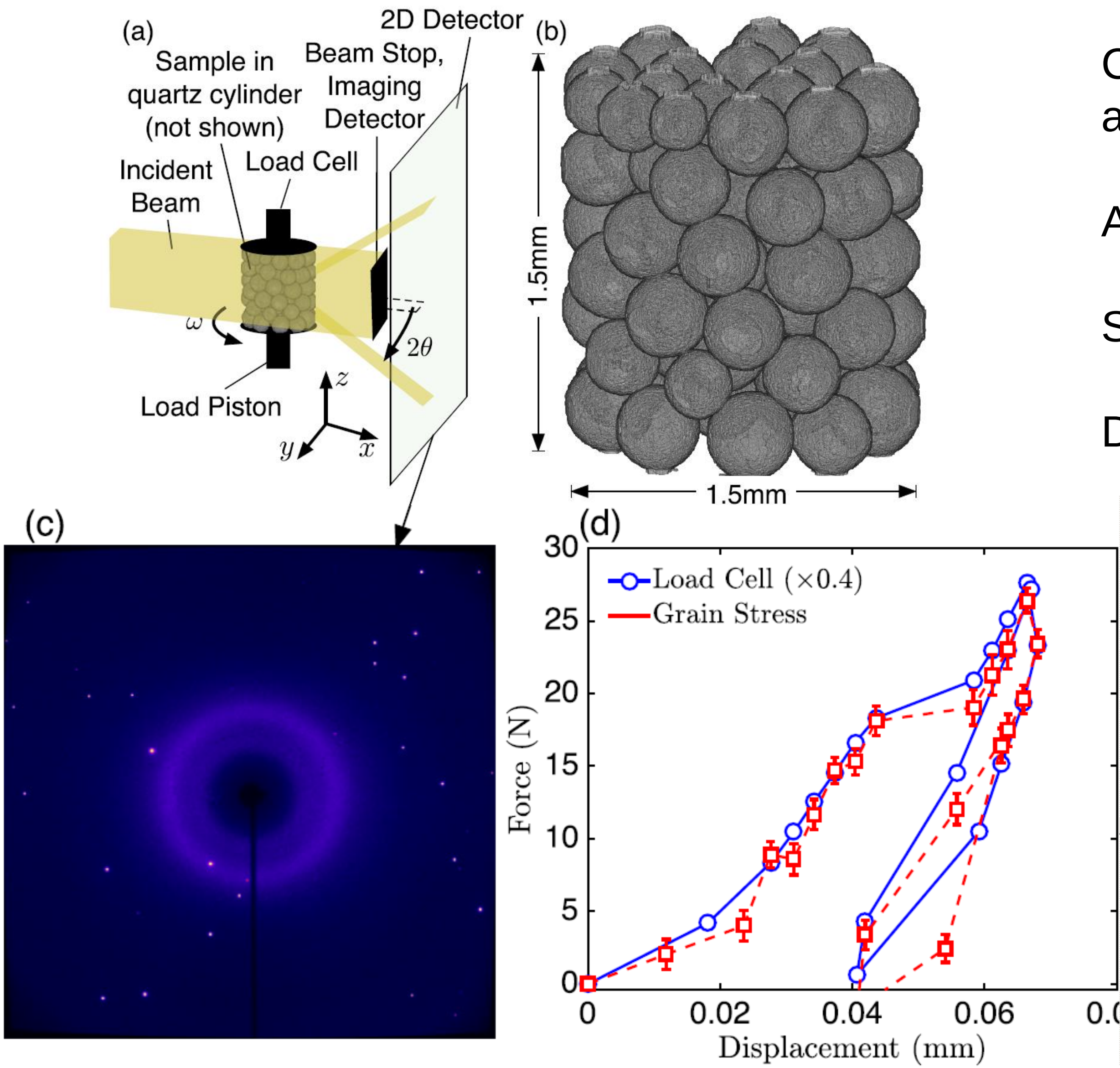

Combined tomography and diffraction

Analysis of strain tensors

Solve inversion problem

Determined contact forces

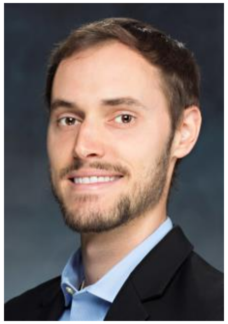

Strain tensors of the quartz grains versus applied load.

Quantitative mechanical force
Information

Color represents strain tensors
Mapped onto surface of grains

32 grains.

Geotechnique Letters ***5*** *236 2015*

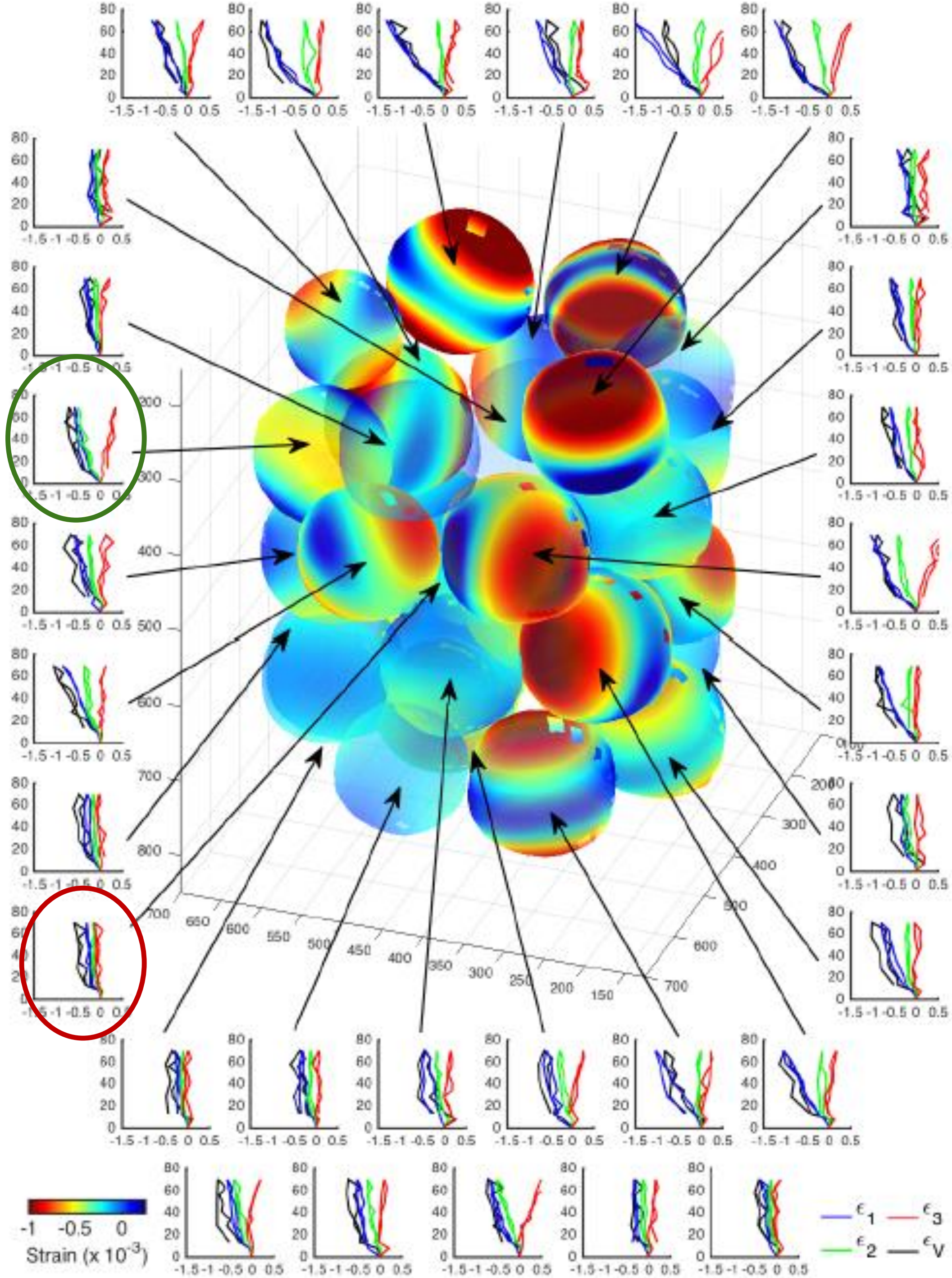

3D EXPERIMENTAL GRANULAR MECHANICS

Stephen A. Hall

Division of Solid Mechanics, Lund University, Lund, Sweden & European Spallation Source AB, Lund, Sweden , stephen.hall@solid.lth.se

Jonathan Wright

European Synchrotron Radiation Facility, Grenoble, France, wright@esrf.fr

EBS:

More accurate strains
Smallest tomo pixel sizes

Nanofocus endstation

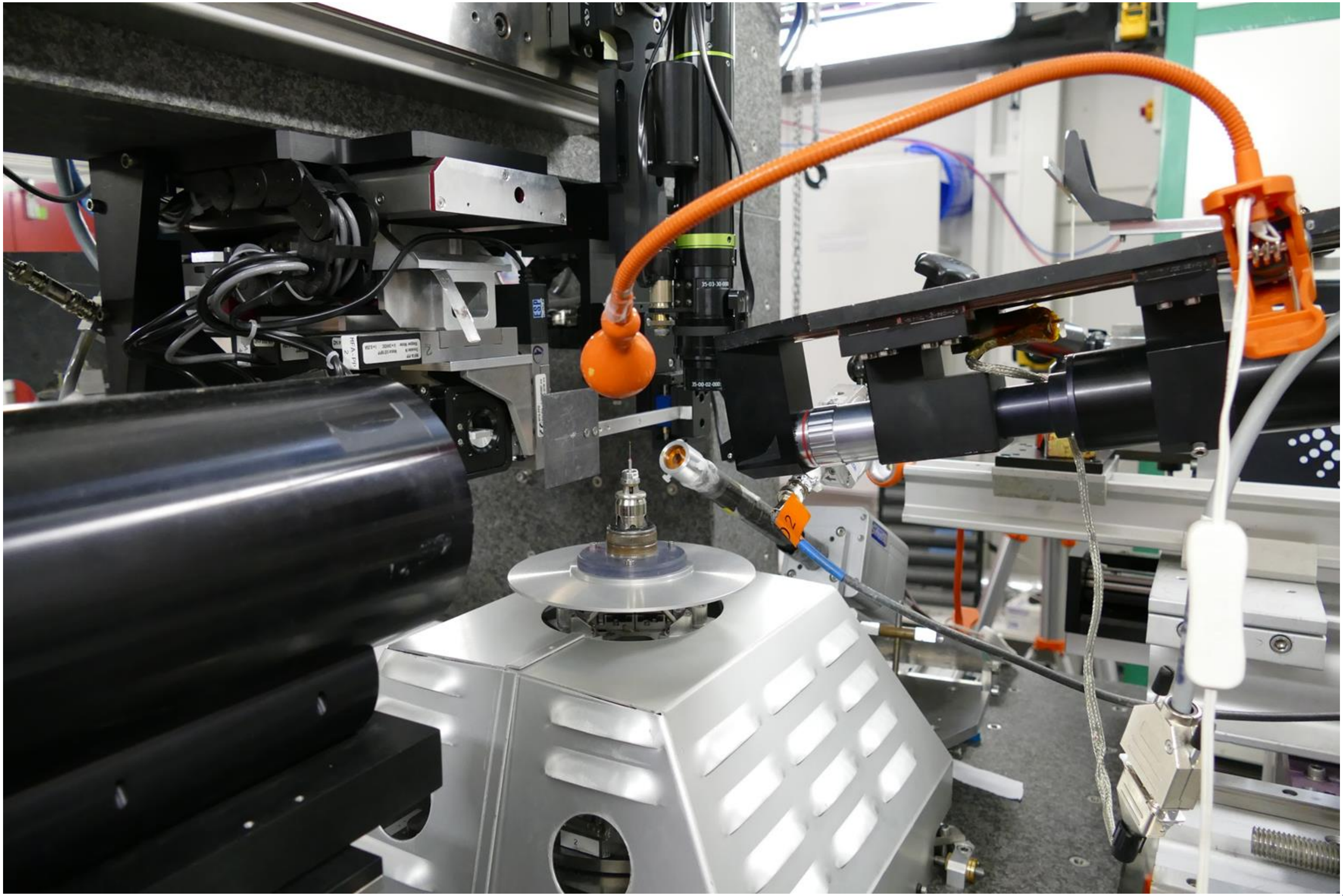

II. Design architecture – ID11 Nanoscope end-station

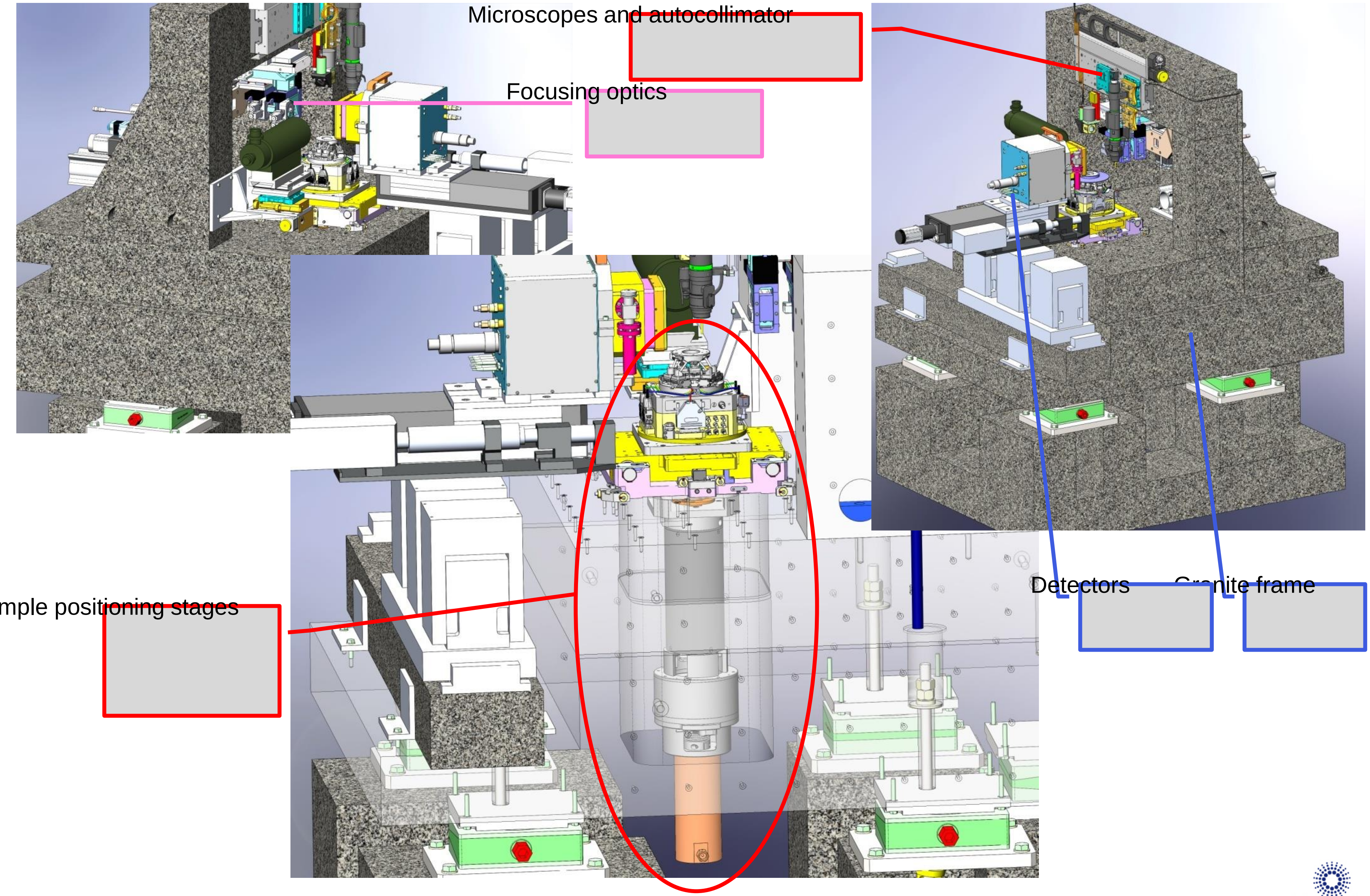

The measurement of stress and phase fraction distributions in pre and post-transition Zircaloy oxides using nano-beam synchrotron X-ray diffraction

H. Swan [a], M.S. Blackmur [a], J.M. Hyde [a,*], A. Laferrere [f], S.R. Ortner [a], P.D. Styman [a], C. Staines [b], M. Gass [c], H. Hulme [c], A. Cole-Baker [d], P. Frankel [e]

Journal of Nuclear Materials 479 (2016) 559–575

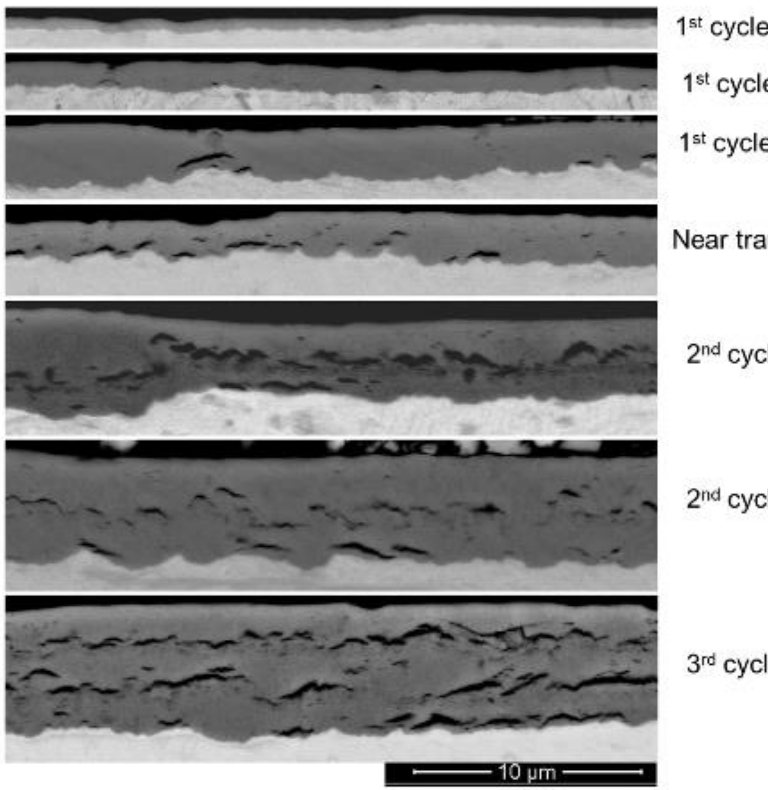

Fig. 9. SEM images of the samples studied, showing the development of undulations and isolated cracks and subsequently, bands of interlinked lateral cracking.

H. Swan et al. / Journal of Nuclear Materials 479 (2016) 559–575

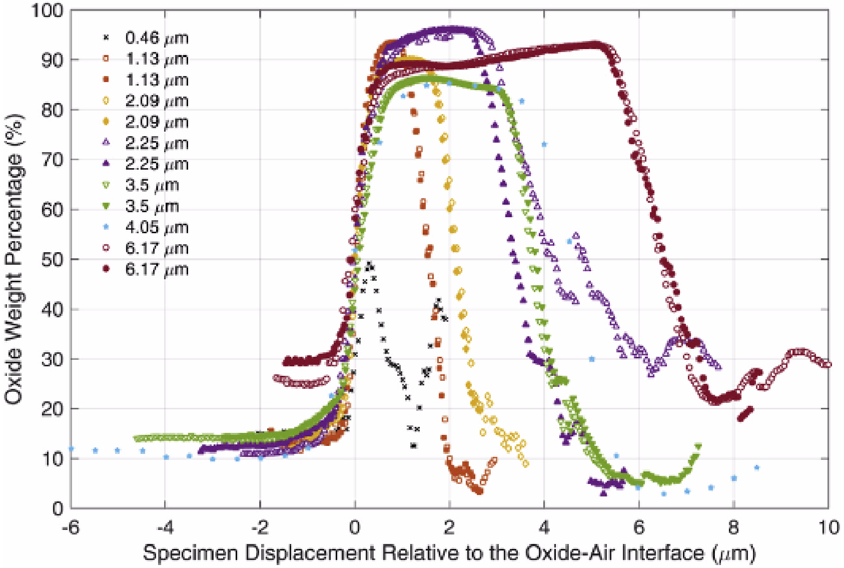

Fig. 4. Oxide entry-exit curves for all samples, offset such that the nominal surface of the oxide is at 0 µm depth.

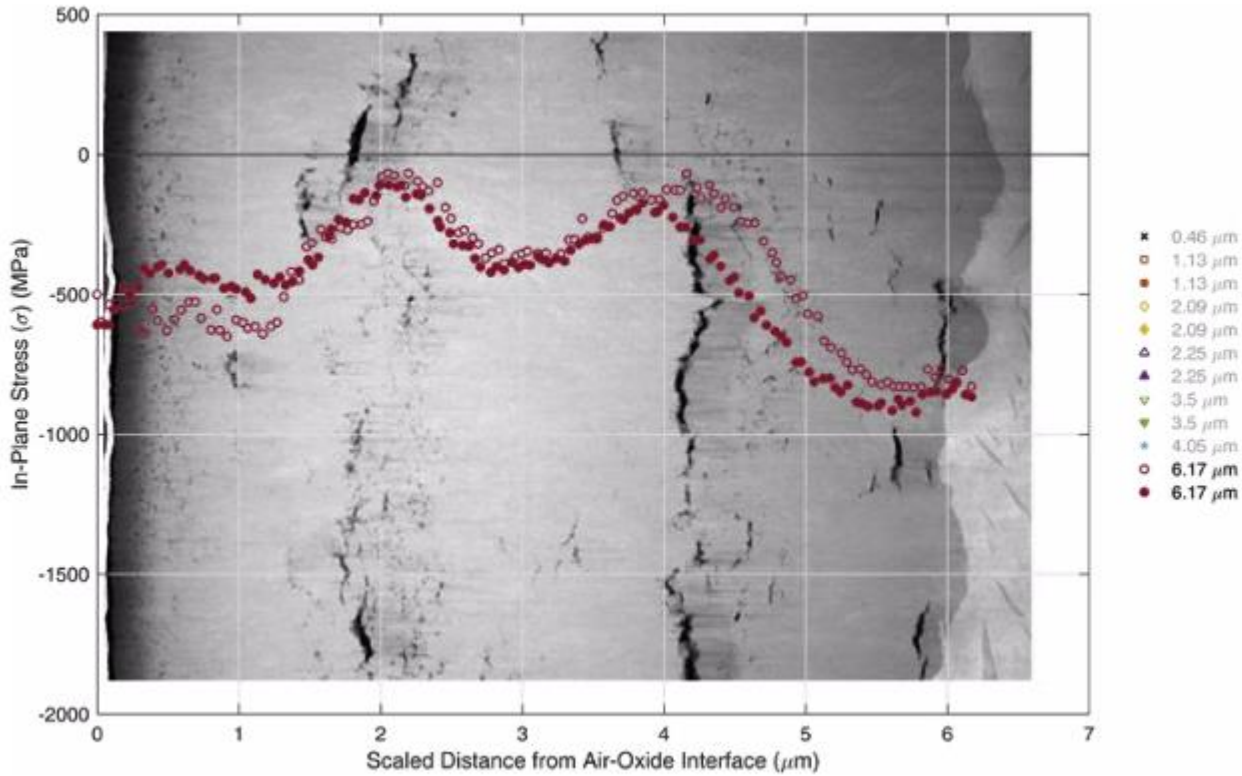

Fig. 10. Correlation between stresses determined from transmission XRD and the crack distribution observed with Scanning Transmission Electron Microscopy in the same sample.

6. Conclusions

Nano-focus transmission XRD has been used for the first time to study the distribution with oxide depth of stresses and tetragonal:monoclinic phase fractions in Zircaloy oxides, without the need for complex deconvolution methods. In contrast to methods such as polychromatic energy-dispersive XRD, or grazing incidence XRD, which provide averages of the stresses and phase fractions that are strongly weighted toward the surface values, the use of a nano-focussed beam has enabled the stress and phase fraction distributions with depth and time to be measured directly with nano-scale resolution. It has therefore been possible to discern non-monotonic changes in the in-plane and through-plane stress distributions and tetragonal:monoclinic weight phase ratios. It has also been possible to relate these physical changes in the oxide to the oxidation rate, in

Tomography has no phase problem…

Fig. 3.6: *The Fourier Slice Theorem relates the Fourier transform of a projection to the Fourier transform of the object along a radial line. (From [Pan83].)*

The Fourier transform of a parallel projection of an image $f(x, y)$ taken at angle θ gives a slice of the two-dimensional transform, $F(u, v)$, subtending an angle θ with the u-axis. In other words, the Fourier transform of $P_\theta(t)$ gives the values of $F(u, v)$ along line BB in Fig. 3.6.

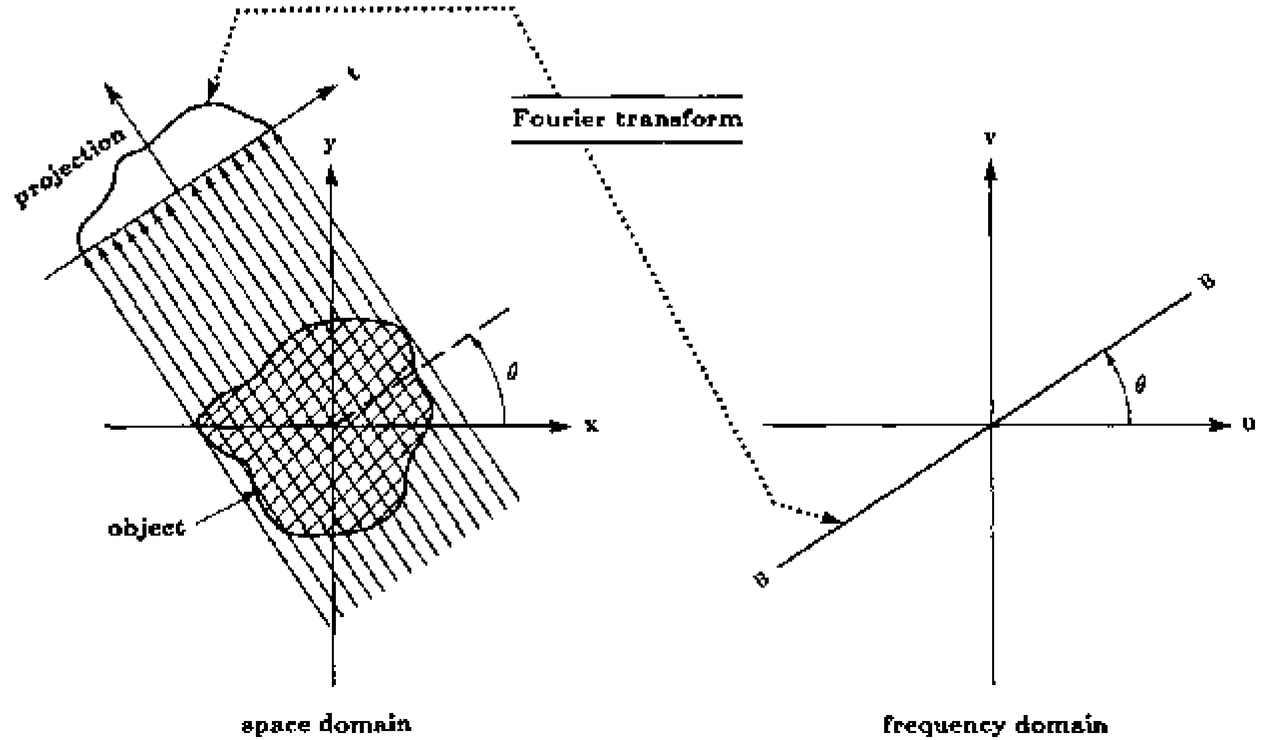

Diffraction based imaging

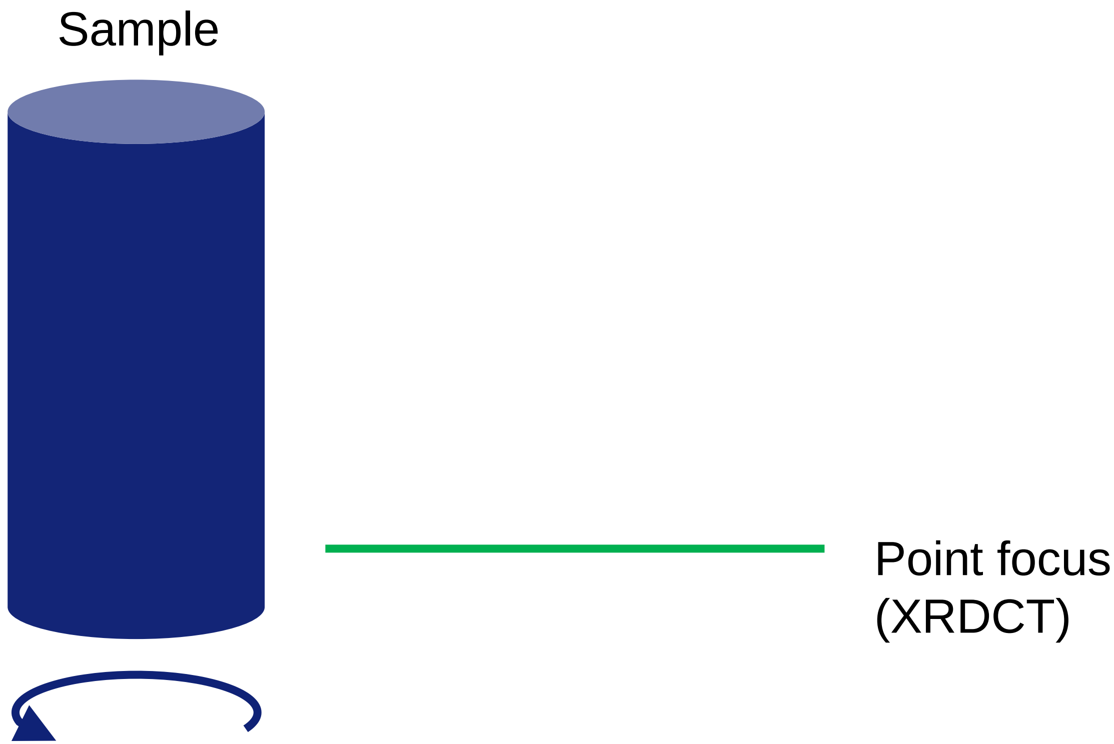

XRD-CT Powders, Nanoparticles, PDF’s

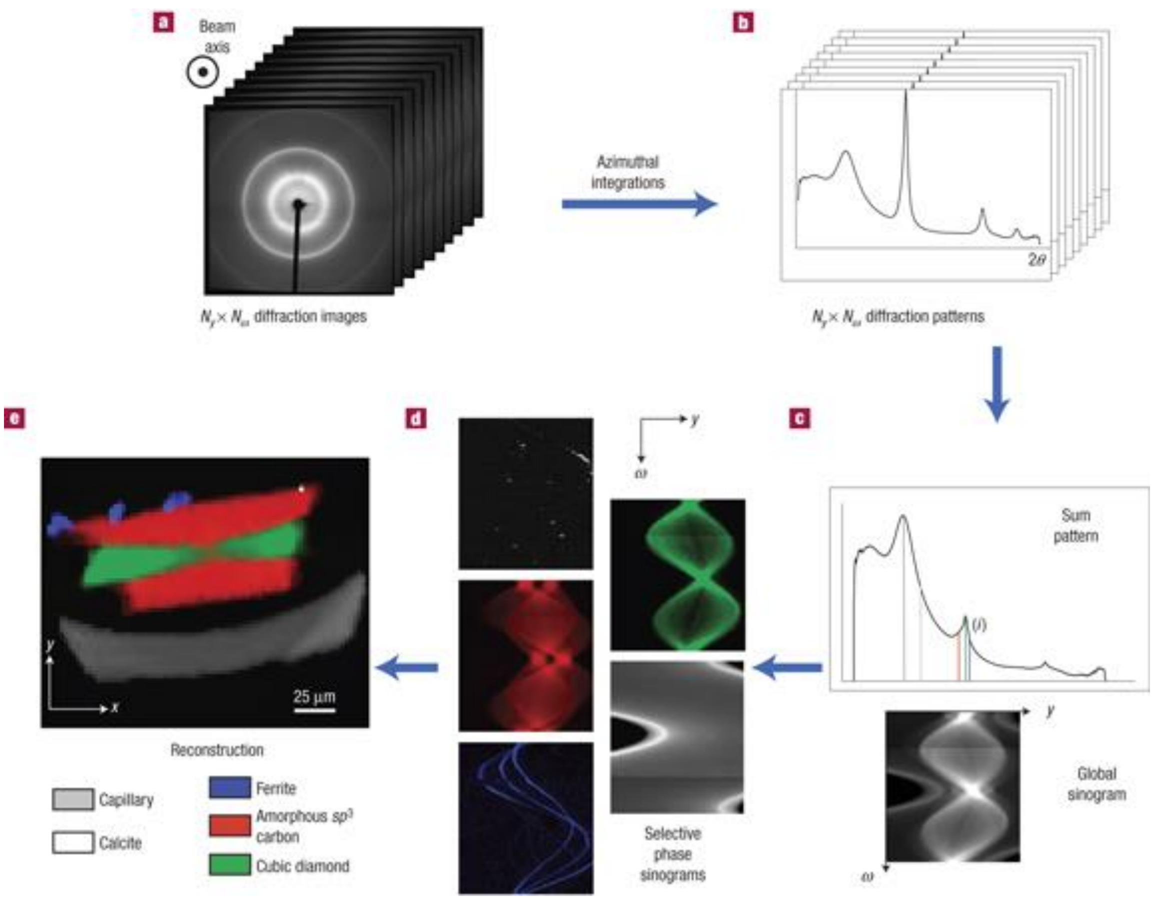

Probing the structure of heterogeneous diluted materials by diffraction tomography

Pierre Bleuet, Eléonore Welcomme, Eric Dooryhée, Jean Susini, Jean-Louis Hodeau & Philippe Walter

Nature Materials **7**, 468 - 472 (2008) Published online: 20 April 2008

doi:10.1038/nmat2168

Dynamic X-ray diffraction computed tomography reveals real-time insight into catalyst active phase evolution, S.D.M. Jacques (a,b), M. di Michiel (c), A.M. Beale (a), T. Sochi (b), M.G. O'Brien (a), L. Espinosa-Alonso (a), B.M. Weckhuysen (a) and P. Barnes (b), ***Angew. Chem. Int. Ed.* 50, 10148 (2011)**;

Active phase evolution in single Ni/Al_2O_3 methanation catalyst bodies studied in real time using combined μ-XRD-CT and μ-absorption-CT, M.G. O'Brien (a), S.D.M. Jacques (a,b), M. di Michiel (c), P. Barnes (b), B.M. Weckhuysen (a) and A.M. Beale (a) *Chem. Sci.* (2011); **DOI: 10.1039/C1SC00637A**.

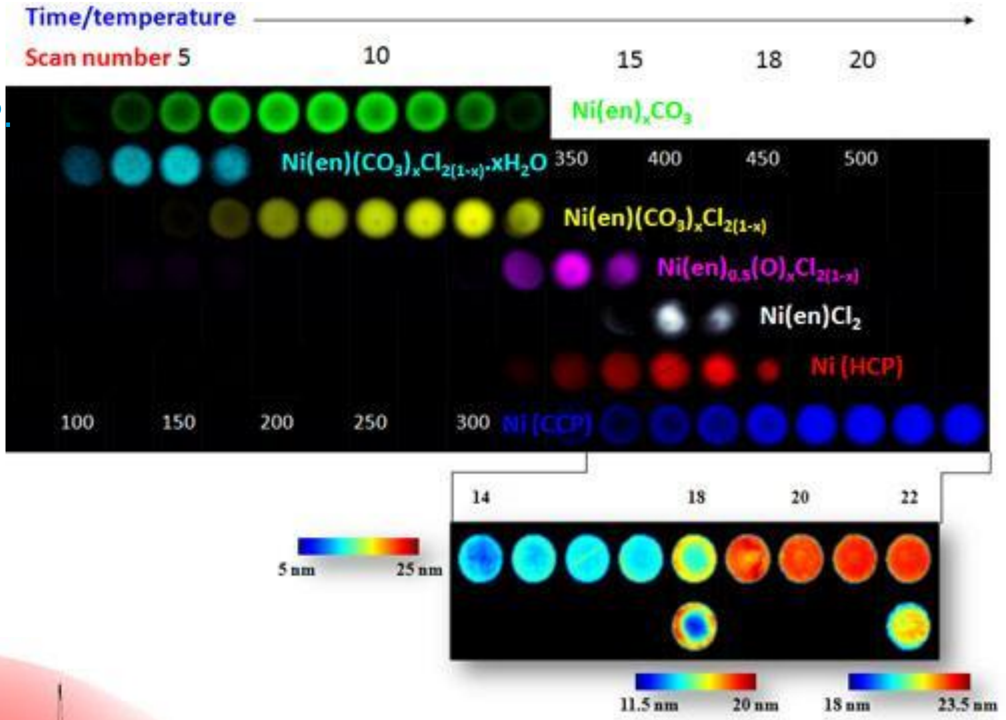

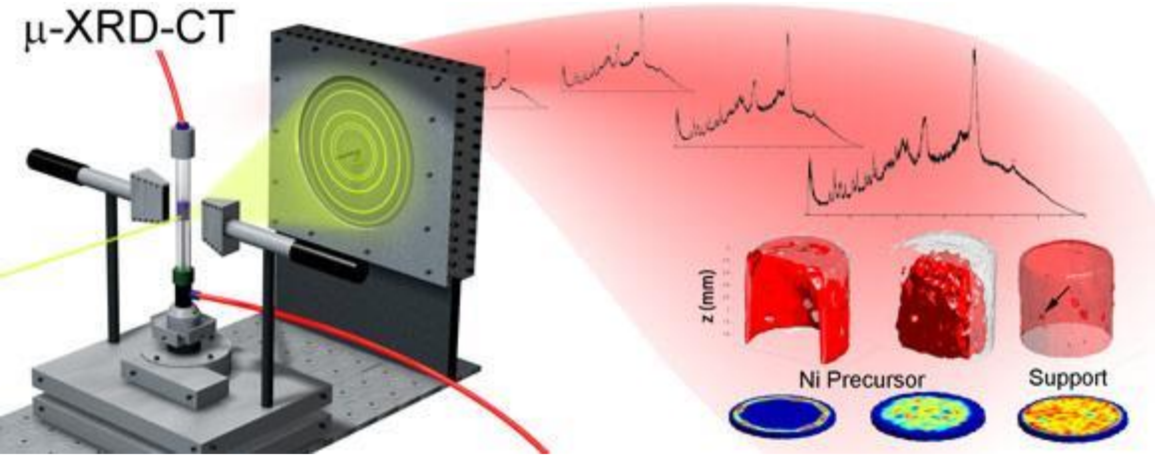

Diffraction tomography: Impurities in UMo (data from ID22)

Data reduction is well established for powder rings

“Spotty” diffraction patterns are more challenging to reconstruct.

Indexing of single grains has been achieved, showing orientation relations of phases

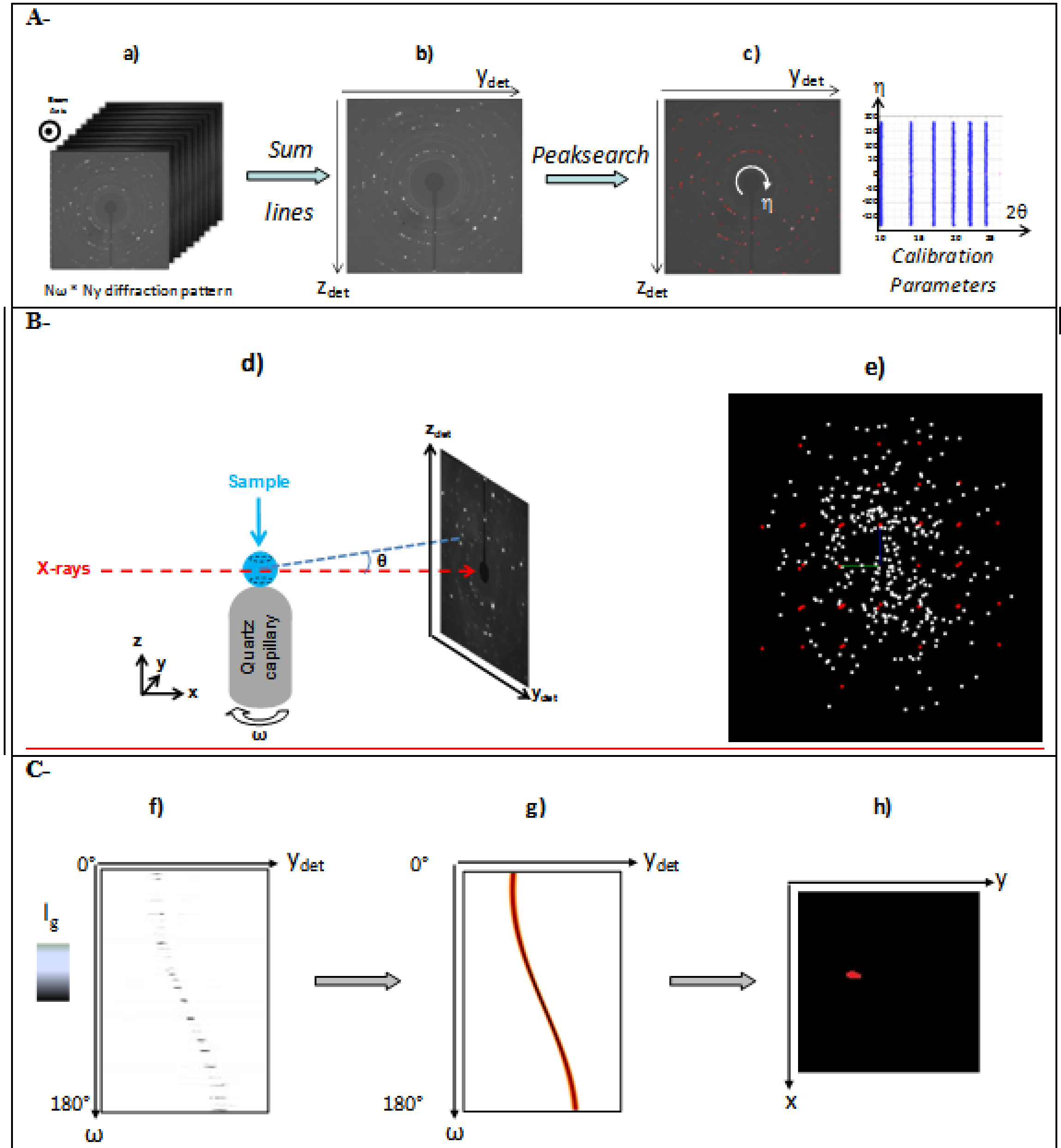

Impurity precipitation in atomized particles evidenced by high resolution diffraction tomography

Anne Bonnin, Jonathan Wright, Rémi Tucoulou, and Hervé Palancher
APPLIED PHYSICS LETTERS 104, 121910 (2014)

Index individual spots and reconstruct grain shapes

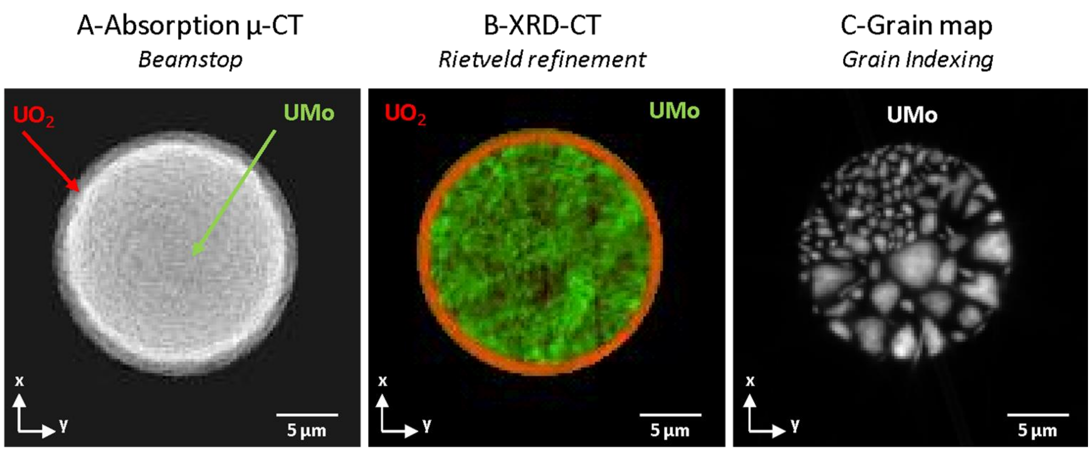

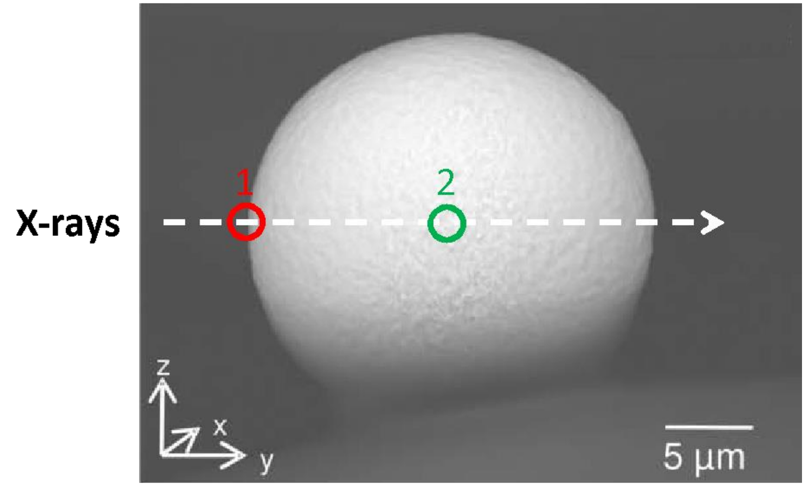

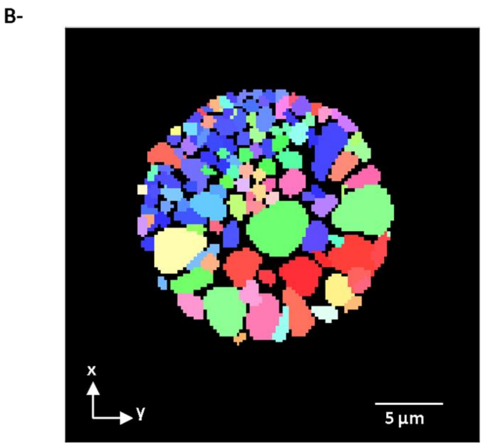

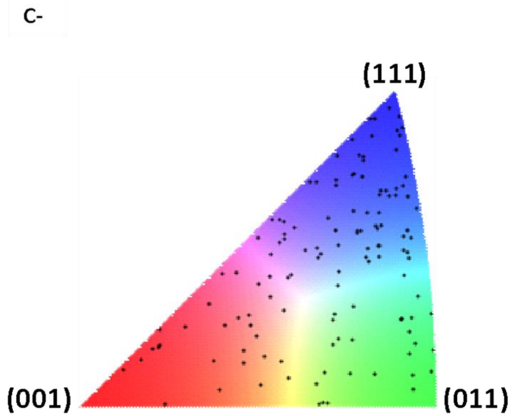

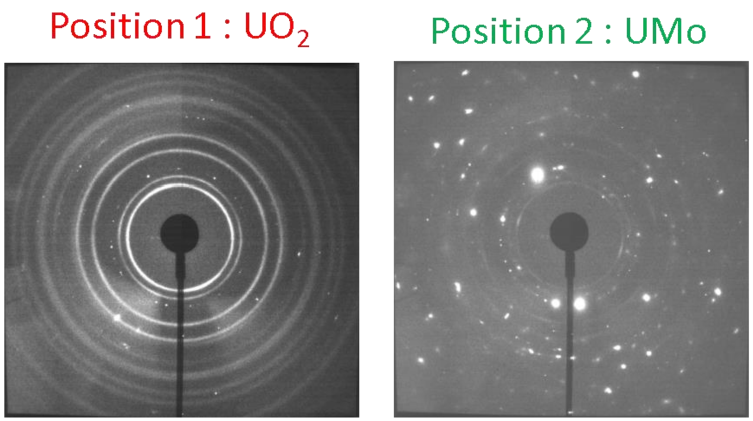

Impurity precipitation in atomized particles evidenced by high resolution diffraction tomography
Anne Bonnin, Jonathan Wright, Rémi Tucoulou, and Hervé Palancher,
APPLIED PHYSICS LETTERS 104, 121910 (2014)

Trace impurity phase mapped out

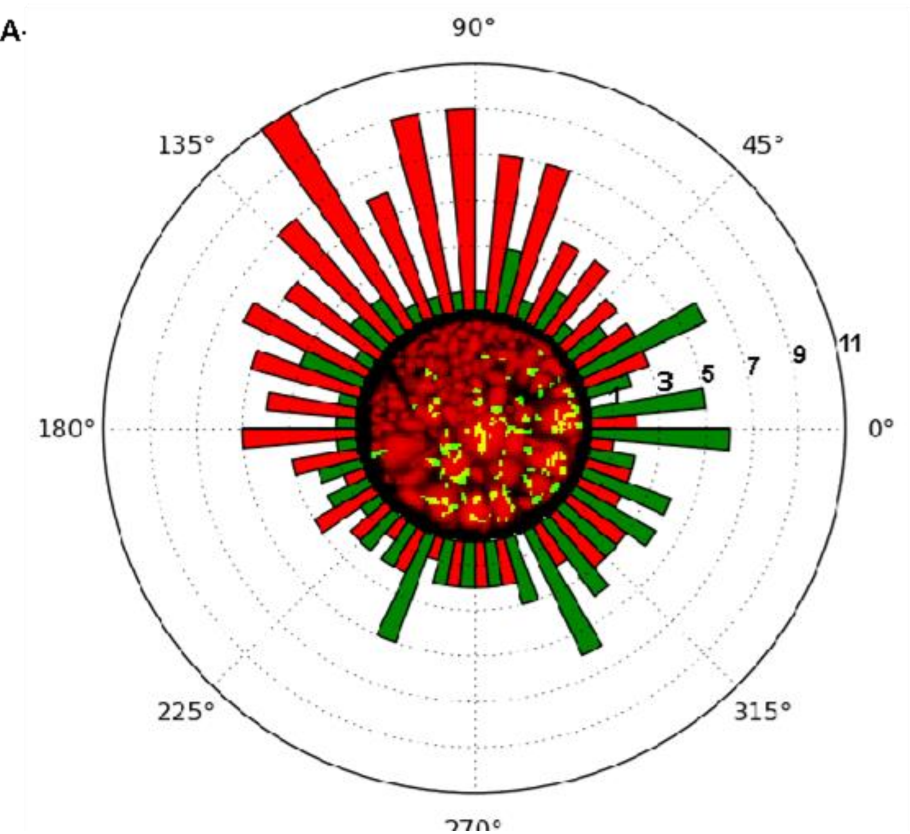

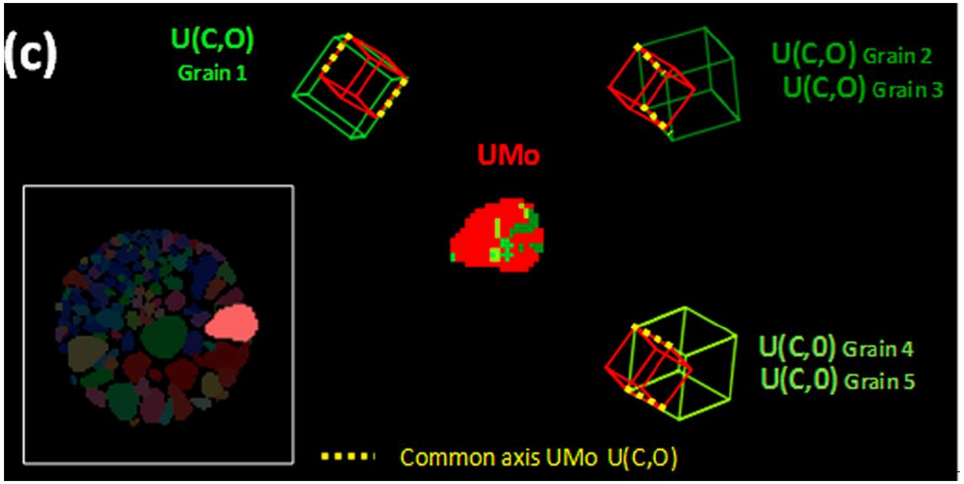

1 wt% impurity phase
Clear orientation relationship between U(C,O) and UMo
Multiple U(C,O) domains in single UMo grain
Mainly found in larger UMo grains

Impurity precipitation in atomized particles evidenced by high resolution diffraction tomography
Anne Bonnin, Jonathan Wright, Rémi Tucoulou, and Hervé Palancher,
APPLIED PHYSICS LETTERS 104, 121910 (2014)

Similar grain in DCT experiment at ID11

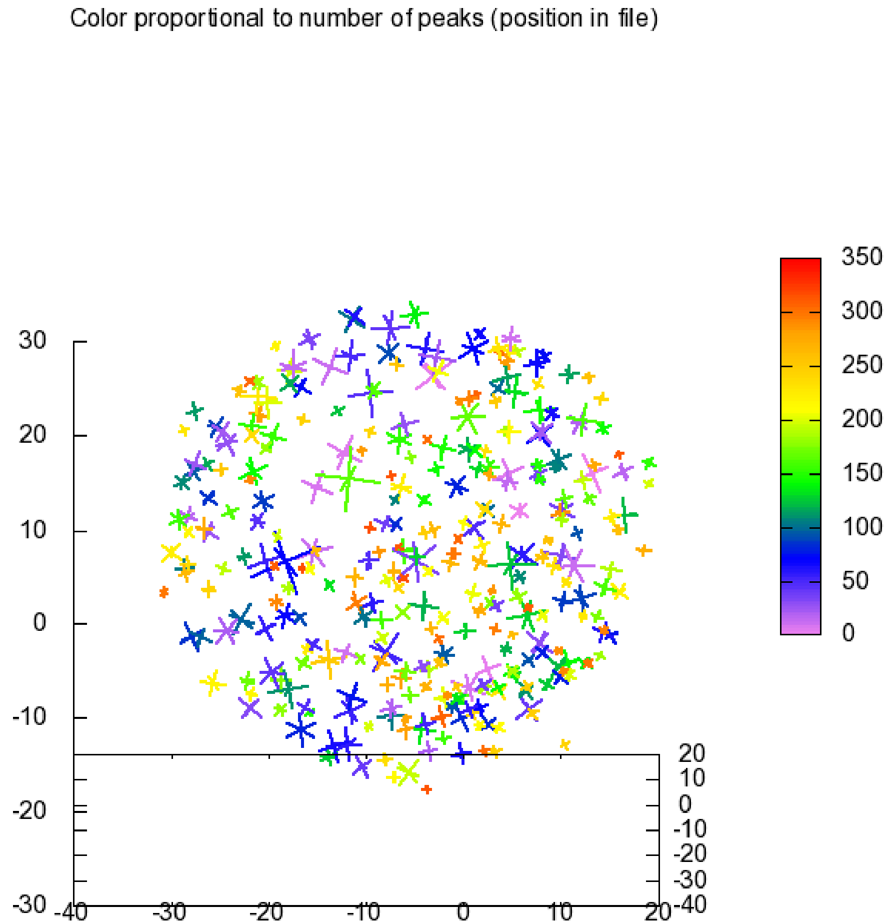

ID11 near-field data
Processed for grain centre of mass

LARGE beamsize

ESRF Upgrade Phase II : new machine

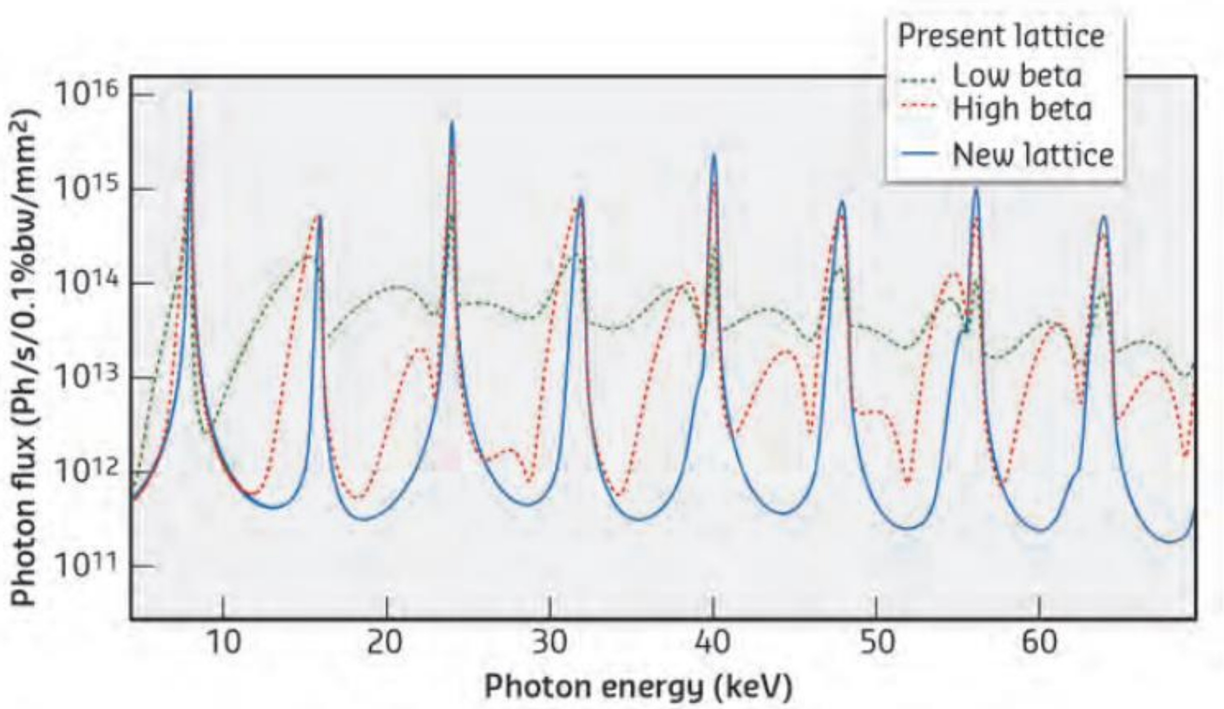

Figure 2.06: Spectral photon flux density (log scale) at 30 m from the source for a 4 m-long CPMU18 (gap 6 mm, K=1.68) for the present and new lattices.

~40X more photons at ID11 after CRL optics

Cleaner spectrum (no need for monochromator?)

LaB6 in broader bandpass X-ray beam

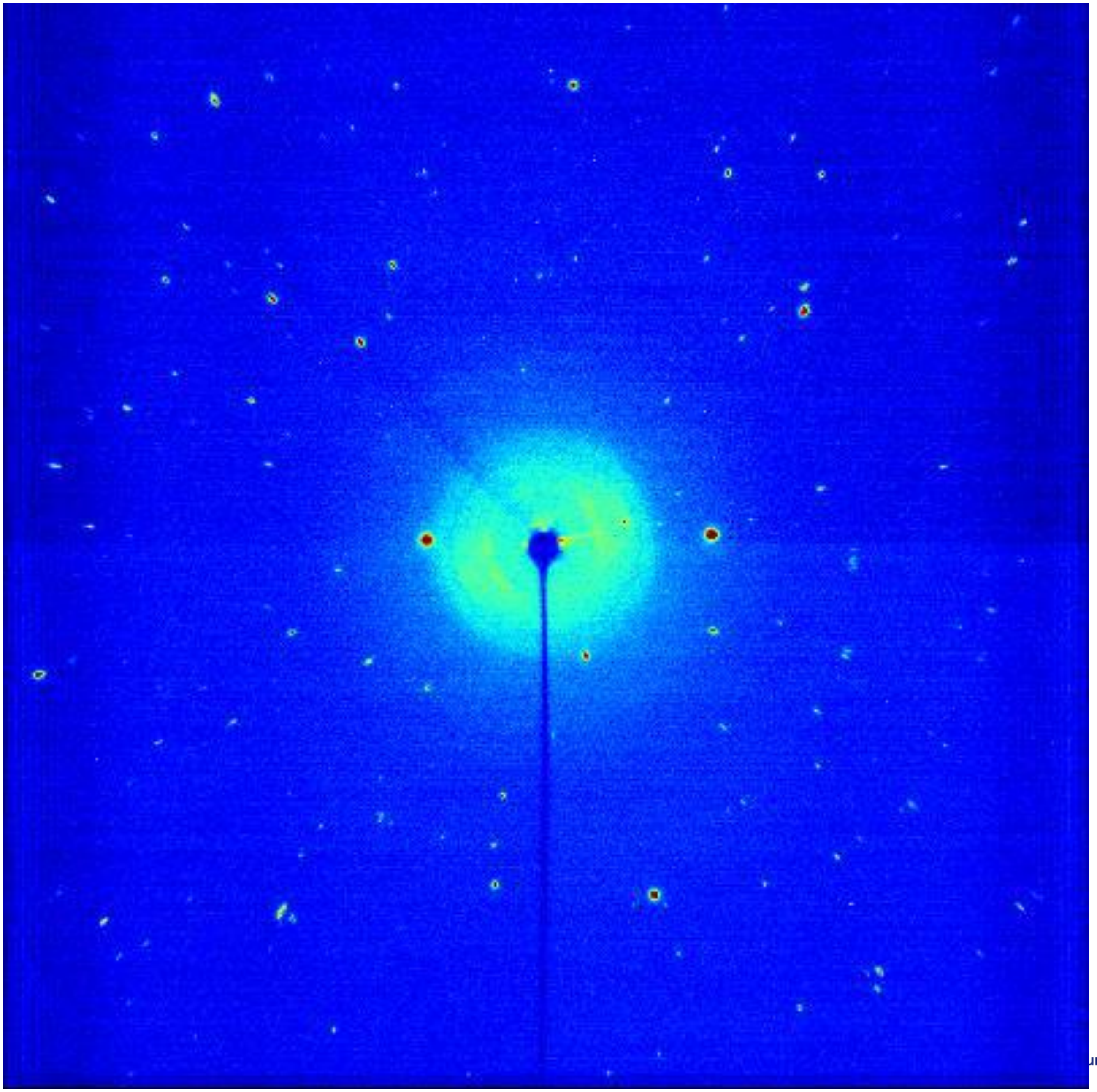

Thanks to our collaborators and beamline users who did the work that was presented here

Thankyou for listening

Line focus X-ray beam example…

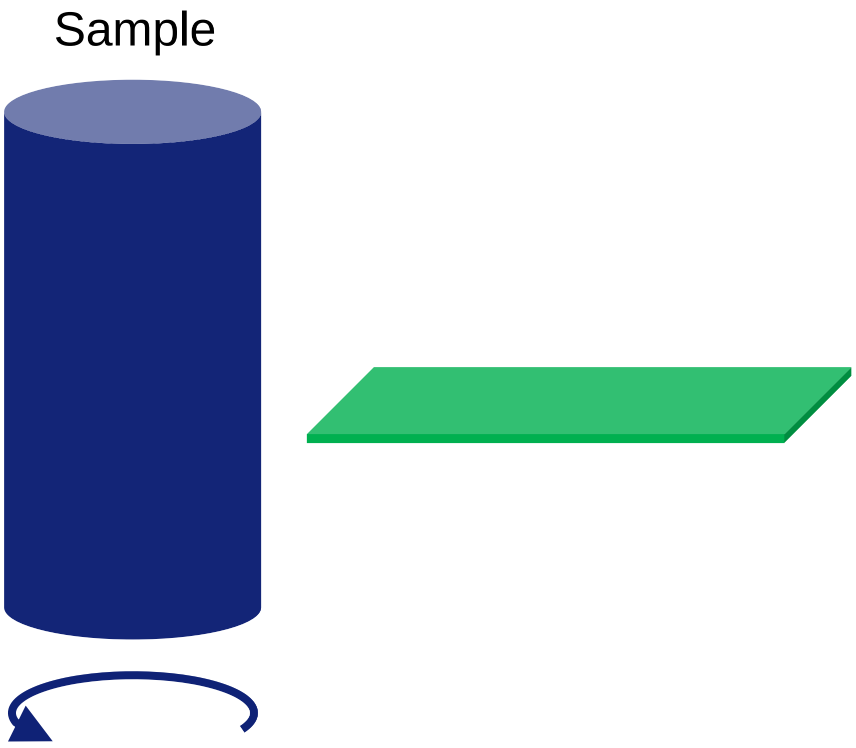

Mapping strains in shape memory alloy

REPORTS

SHAPE-MEMORY ALLOYS

Grain-resolved analysis of localized deformation in nickel-titanium wire under tensile load

P. Sedmák,[1,2] J. Pilch,[1] L. Heller,[1] J. Kopeček,[1] J. Wright,[3] P. Sedlák,[4] M. Frost,[4] P. Šittner[1]*

The stress-induced martensitic transformation in tensioned nickel-titanium shape-memory alloys proceeds by propagation of macroscopic fronts of localized deformation. We used three-dimensional synchrotron x-ray diffraction to image at micrometer-scale resolution the grain-resolved elastic strains and stresses in austenite around one such front in a prestrained nickel-titanium wire. We found that the local stresses in austenite grains are modified ahead of the nose cone–shaped buried interface where the martensitic transformation begins. Elevated shear stresses at the cone interface explain why the martensitic transformation proceeds in a localized manner. We established the crossover from stresses in individual grains to a continuum macroscopic internal stress field in the wire and rationalized the experimentally observed internal stress field and the topology of the macroscopic front by means of finite element simulations of the localized deformation.

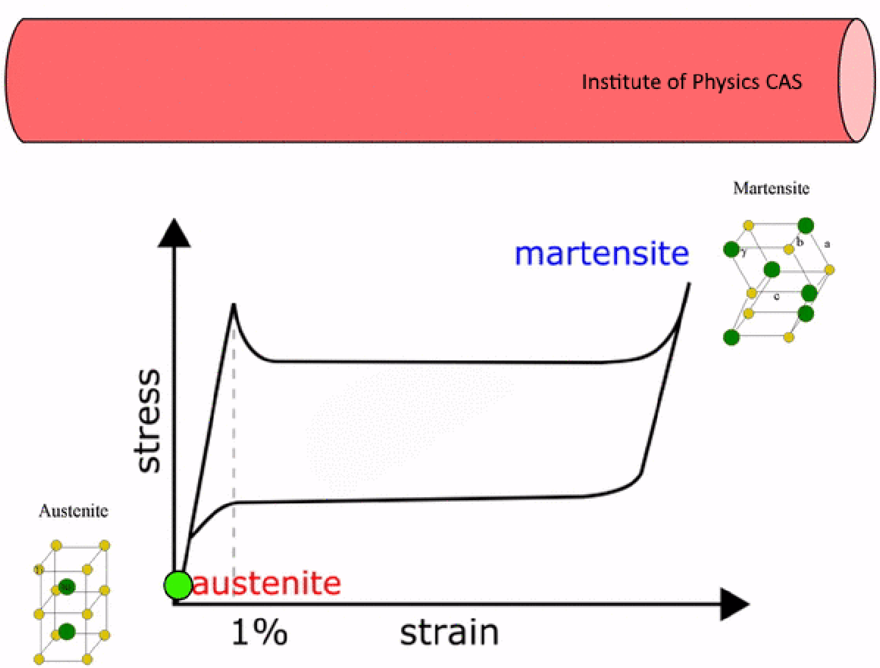

Science (2016) **353** 6299

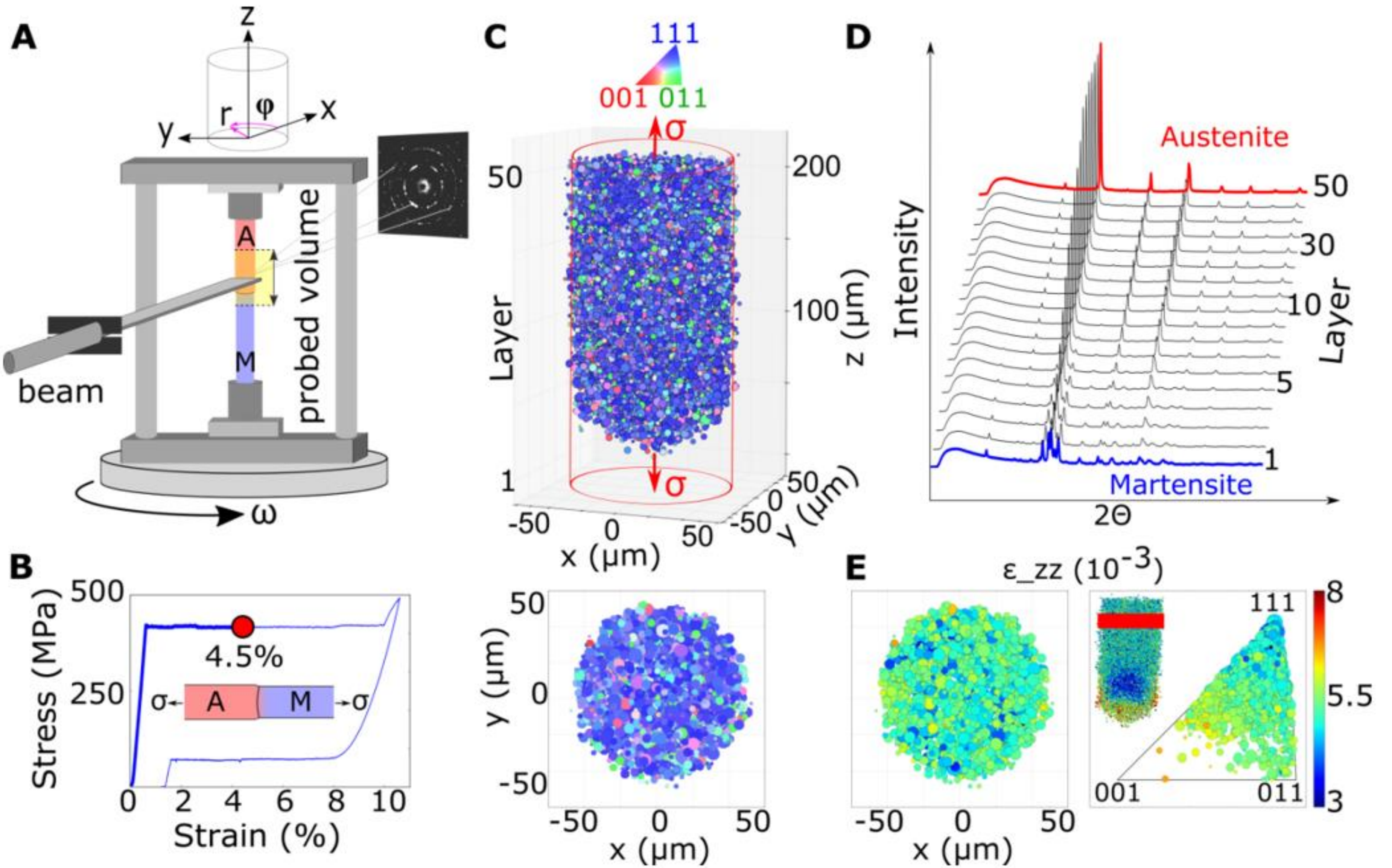
A
z
y
r
φ
x
A
M
probed volume
beam
ω
B
Stress (MPa)
500
250
4.5%
σ
A
M
σ
0
2
4
6
8
10
Strain (%)
C
111
001 011
σ
σ
50
1
Layer
200
100
z (µm)
-50
0
50
x (µm)
y (µm)
D
Intensity
Austenite
50
30
10
5
1
Layer
Martensite
2Θ
E
ε_zz (10-3)
111
001
011
8
5.5
3

Comparison to EBSD

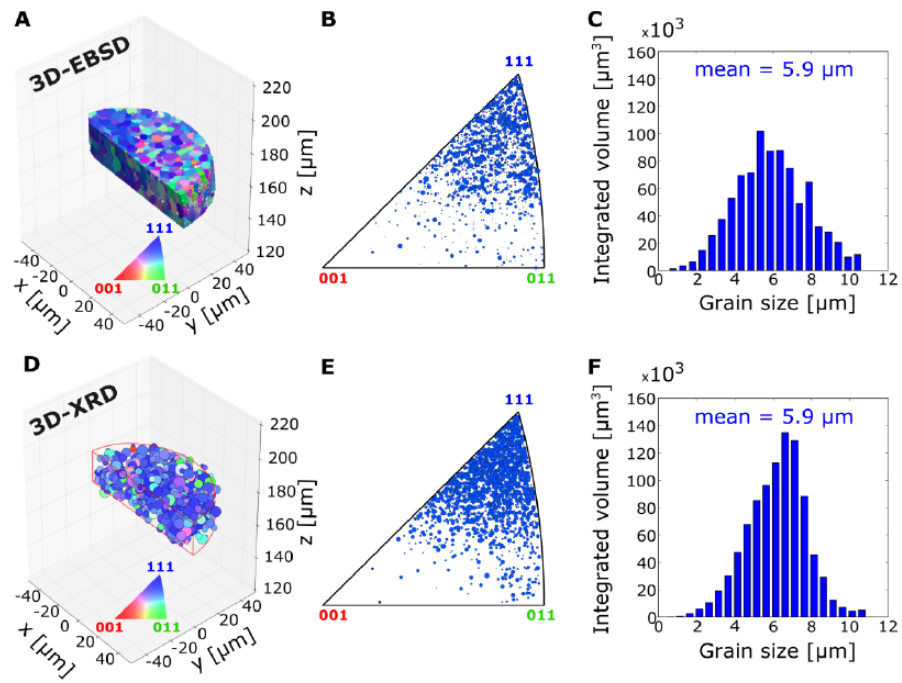

Fig. S4:

3D rendering of shear stress

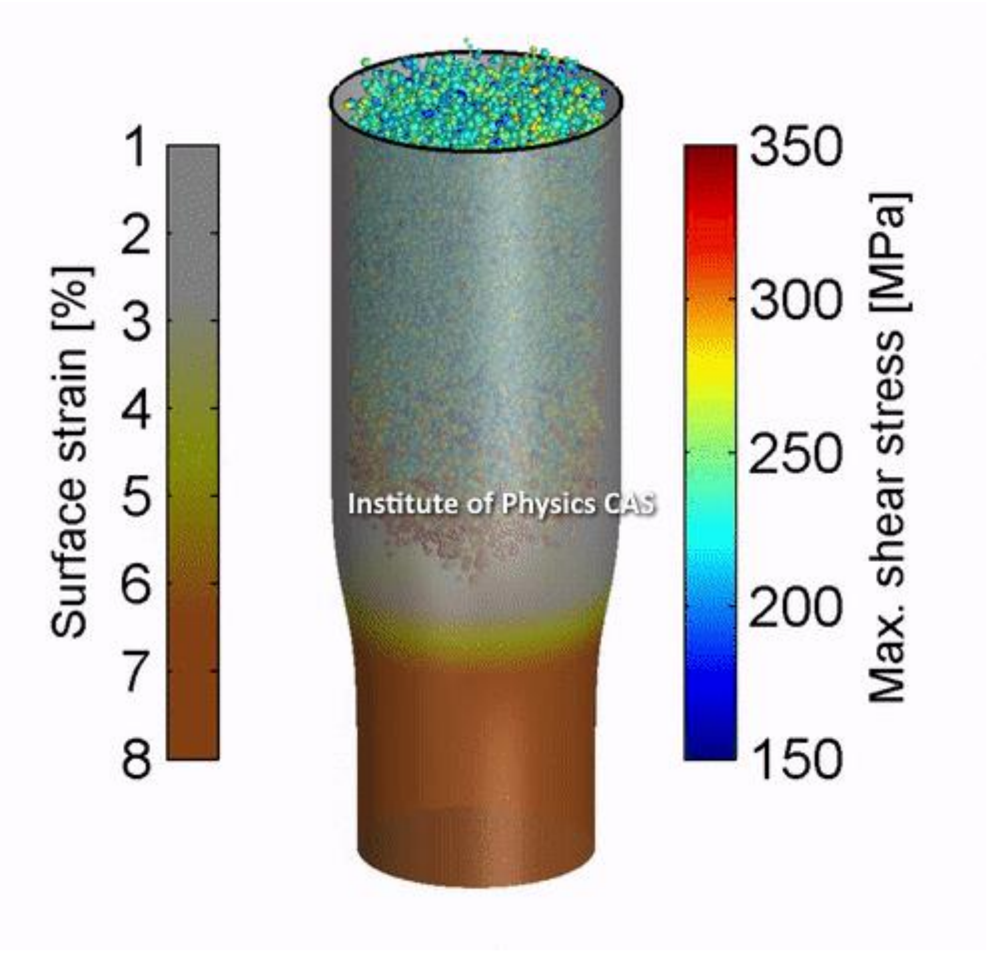

3D strain tensors at the martensite band front

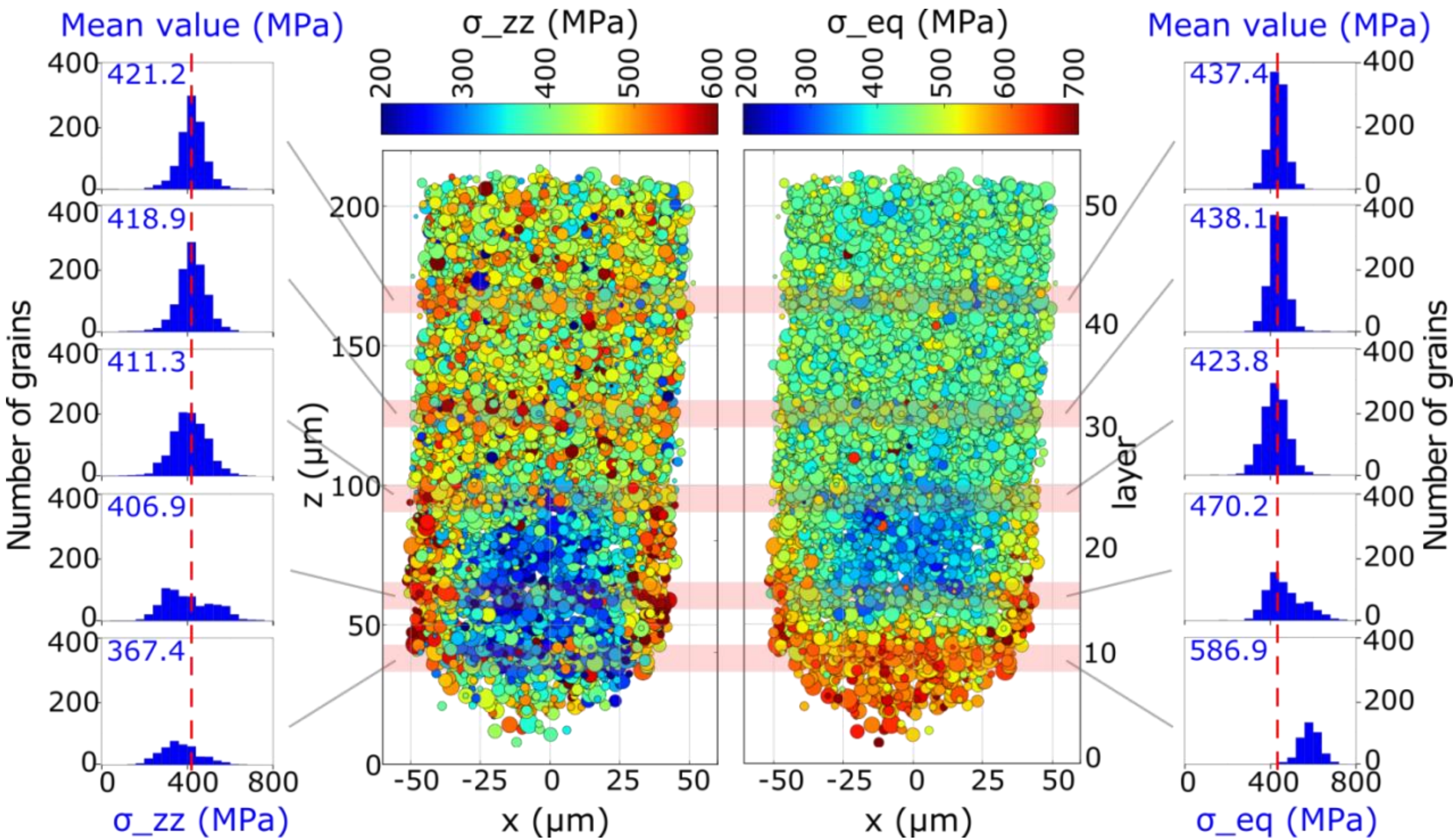

The European Synchrotron | ESRF